LETTER

https://doi.org/10.1038/s41586-018-0538-8

# mRNA circularization by METTL3–eIF3h enhances translation and promotes oncogenesis

Junho Choe[1,2,17], Shuibin Lin[1,2,3,17], Wencai Zhang[4], Qi Liu[1,2], Longfei Wang[2], Julia Ramirez-Moya[1,5], Peng Du[1,2], Wantae Kim[6,16], Shaojun Tang[7,8], Piotr Sliz[2], Pilar Santisteban[5], Rani E. George[9,10], William G. Richards[11], Kwok-Kin Wong[12], Nicolas Locker[13], Frank J. Slack[4,14,15] & Richard I. Gregory[1,2,10,14,15]*

***N*$^6$-methyladenosine ($m^6A$) modification of mRNA is emerging as an important regulator of gene expression that affects different developmental and biological processes, and altered $m^6A$ homeostasis is linked to cancer[1–5]. $m^6A$ modification is catalysed by METTL3 and enriched in the 3′ untranslated region of a large subset of mRNAs at sites close to the stop codon[5]. METTL3 can promote translation but the mechanism and relevance of this process remain unknown[1]. Here we show that METTL3 enhances translation only when tethered to reporter mRNA at sites close to the stop codon, supporting a mechanism of mRNA looping for ribosome recycling and translational control. Electron microscopy reveals the topology of individual polyribosomes with single METTL3 foci in close proximity to 5′ cap-binding proteins. We identify a direct physical and functional interaction between METTL3 and the eukaryotic translation initiation factor 3 subunit h (eIF3h). METTL3 promotes translation of a large subset of oncogenic mRNAs—including bromodomain-containing protein 4—that is also $m^6A$-modified in human primary lung tumours. The METTL3–eIF3h interaction is required for enhanced translation, formation of densely packed polyribosomes and oncogenic transformation. METTL3 depletion inhibits tumorigenicity and sensitizes lung cancer cells to BRD4 inhibition. These findings uncover a mechanism of translation control that is based on mRNA looping and identify METTL3–eIF3h as a potential therapeutic target for patients with cancer.**

Despite awareness of the biological importance of $m^6A$ in various organisms, the mechanisms by which $m^6A$ regulates gene expression remain poorly understood. Proteins that contain YTH domains can specifically bind $m^6A$-modified RNA to regulate mRNA splicing, export, stability and translation[5–8]. In addition, we found that tethering METTL3 to mRNA reporters promotes translation and METTL3 enhances translation of oncogenes including *EGFR* in human lung cancer cells[1].

The initiation step of translation is rate limiting and a closed-loop model was proposed to facilitate multiple rounds of mRNA translation. This is supported by functional and physical interaction between the capped 5′ terminus and the polyadenylated 3′ terminus of mRNA mediated by the translation initiation factor eIF4G and PABPC1 (poly(A) binding protein cytoplasmic 1)[9–12]. Our data support an alternative closed-loop model, in which circularization of the mRNA is mediated by association between the eIF3h subunit at the 5′-end of the mRNA and METTL3 bound to specific sites near the translation stop codon. We find that METTL3 promotes translation of a large subset of oncogenic mRNAs and that METTL3–eIF3h interaction is required for oncogenic transformation. These findings provide new insights into the mechanism of translation control and suggest that METTL3–eIF3h and downstream oncogenes could be therapeutic targets for cancer.

To test a mRNA-looping model we first examined whether the METTL3-binding position on mRNA is important for its ability to enhance translation. Using reporters with MS2-binding sites located at different positions (Extended Data Fig. 1a), we found that direct METTL3 tethering can promote translation only when bound to the 3′ untranslated region (UTR) at a position near the stop codon. In vitro translation assays performed with cell lysates, recombinant METTL3 protein and in vitro-transcribed mRNAs confirmed that full-length METTL3 or an amino-terminal fragment (1–200 amino acids (a.a.)) that is sufficient to promote reporter translation in cells (Extended Data Fig. 2) enhanced translation of a luciferase reporter mRNA (Extended Data Fig. 1e–g). METTL3 tethering had a stronger effect on mRNAs that lack a poly(A) tail (Extended Data Fig. 1g), which is consistent with some redundancy between METTL3 and eIF4G–PABPC1-mediated looping for mRNAs with poly(A) tails in these in vitro assays.

To provide evidence that METTL3 is bound to polyribosomes, mRNA ribonucleoprotein complexes (mRNPs) containing Flag–METTL3 were affinity purified, incubated with gold-labelled anti-METTL3 antibodies, subjected to sucrose gradient fractionation and then analysed by electron microscopy (Fig. 1a). This revealed gold-labelled METTL3 in the individual polyribosomes (Extended Data Fig. 4a, b). We performed similar experiments using either anti-CBP80 or anti-eIF4E gold-labelled antibodies together with the anti-METTL3 particles. As the anti-CBP80 and anti-eIF4E gold particles were larger, they could be distinguished from the anti-METTL3 particles. Individual polyribosomes containing double-labelled gold particles showed that each METTL3 signal is in close proximity (less than 20 nm) to a cap-binding protein (Fig. 1b, Extended Data Fig. 4c, d). This reveals the topology of individual endogenous METTL3-bound polyribosomes and supports the notion that METTL3 mediates the looping of mRNA to promote efficient translation.

Full-length METTL3 as well as the 1–200 a.a. and 1–350 a.a. fragments were found to associate with $m^7$GTP-agarose in cap-binding assays (Extended Data Fig. 3a). This result is highly consistent with tethering assays (Extended Data Fig. 2) and supports the notion that the 1–200 a.a. fragment of METTL3 interacts with translation initiation factor(s) to promote translation. Knockdown of METTL3 had no effect on the association of cap-binding proteins or translation initiation factors (Extended Data Fig. 3b). Thus, formation of the translation initiation complex does not require METTL3. Conversely, the association of METTL3 with $m^7$GTP-agarose was diminished using lysates depleted for CTIF, eIF4GI or eIF3b, supporting the notion that the

[1]Stem Cell Program, Division of Hematology/Oncology, Boston Children's Hospital, Boston, MA, USA. [2]Department of Biological Chemistry and Molecular Pharmacology, Harvard Medical School, Boston, MA, USA. [3]Center for Translational Medicine, The First Affiliated Hospital, Sun Yat-sen University, Guangzhou, China. [4]Department of Pathology, Cancer Center, Beth Israel Deaconess Medical Center, Boston, MA, USA. [5]Instituto de Investigaciones Biomédicas, Consejo Superior de Investigaciones Científicas and Universidad Autónoma de Madrid (CSIC-UAM), Madrid, Spain. [6]Harvard School of Dental Medicine, Boston, MA, USA. [7]Innovation Center for Biomedical Informatics, Georgetown University Medical Center, Washington, DC, USA. [8]Department of Oncology, Lombardi Comprehensive Cancer Center, Georgetown University, Washington, DC, USA. [9]Department of Pediatric Oncology, Dana-Farber Cancer Institute, Boston, MA, USA. [10]Department of Pediatrics, Harvard Medical School, Boston, MA, USA. [11]Department of Surgery, Brigham and Women's Hospital, Boston, MA, USA. [12]Division of Hematology and Medical Oncology, NYU School of Medicine, New York, NY, USA. [13]School of Biosciences and Medicine, University of Surrey, Guildford, UK. [14]Harvard Initiative for RNA Medicine, Boston, MA, USA. [15]Harvard Stem Cell Institute, Cambridge, MA, USA. [16]Present address: Biomedical Translational Research Center, Korea Research Institute of Bioscience and Biotechnology (KRIBB), Daejeon, South Korea. [17]These authors contributed equally: Junho Choe, Shuibin Lin. *e-mail: rgregory@enders.tch.harvard.edu

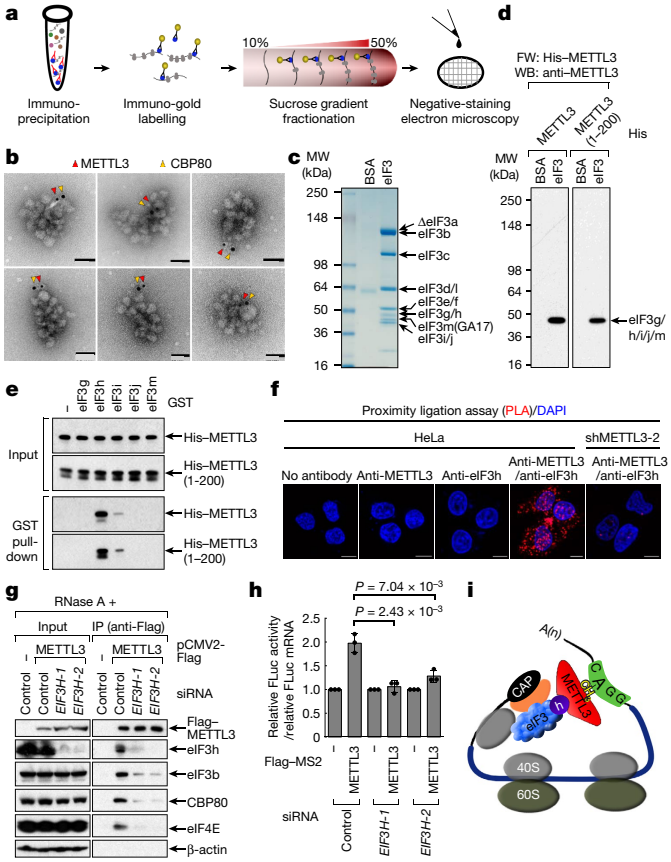


**Fig. 1 | METTL3 enhances translation of target mRNAs by interacting with eIF3h. a**, Electron microscopy procedure. **b**, Electron-microscopy images of polyribosomes. Red arrows, METTL3 with immuno-gold particle (6 nm); yellow arrows, CBP80 with immuno-gold particle (10 nm). Scale bars, 50 nm. Images are representative of three independently performed experiments with similar results. **c**, **d**, Far-western (FW) blot. **c**, Colloidal Coomassie blue staining of eIF3 complex. A breakdown product is denoted (ΔeIF3a). **d**, Far-western blot of purified eIF3 complex. Images are representative of two independently performed experiments with similar results. **e**, GST-tagged eIF3 subunits and co-purified His–METTL3 or 1–200 a.a. analysed by western blotting. Two independently performed experiments show similar results. **f**, Proximity ligation assay. Images are representative of two independently performed experiments with similar results. shMETTL3-2, METTL3 knockdown mediated by shRNA against *METTL3*; -1 and -2 suffixes denote separate identical shRNAs. **g**, Co-immunoprecipitation from control or eIF3h knockdown cells. Images are representative of two independently performed experiments with similar results. IP, immunoprecipitate. **h**, Tethering assays. Data are mean ± s.d. from three biologically independent samples. *P* values are from a two-sided *t*-test. FLuc, firefly luciferase. **i**, Model of METTL3-dependent mRNA translation. CAP, cap; h, eIF3h; GGAC, m6A motif sequence; (A)n, poly(A) tail; siRNA, small interfering RNA; 40S, 40S ribosomal subunit; 60S, 60S ribosomal subunit.

association of METTL3 with m$^7$GTP-agarose is mediated through an interaction with general translation initiation factor(s) (Extended Data Fig. 3c).

A large-scale purification and mass spectroscopy characterization of complexes containing Flag–METTL3 identified numerous translation factors (Extended Data Fig. 3d). Gene Ontology analysis of the METTL3-interacting proteins identified 'mRNA metabolic processes', 'RNA processing' and 'Translation' as the most significantly enriched categories (Extended Data Fig. 3e, f). Considering this and our previous observation that METTL3 knockdown diminishes the association of eIF3 with cap-binding proteins in co-immunoprecipitation, we hypothesized that METTL3 might interact directly with certain component(s) of the multi-subunit eIF3 complex.

To test whether METTL3 interacts with any of the 13 subunit(s) of eIF3, recombinant METTL3 and 1–200 a.a. were used for far-western blotting with a purified human eIF3 complex (Extended Data Fig. 4e, Fig. 1c). METTL3 and 1–200 a.a. both specifically bound to a single band that probably corresponds to eIF3g, eIF3h, eIF3i, eIF3j or eIF3m (Fig. 1d). To further confirm this interaction and to define the particular subunit(s) that interacts with METTL3, we individually expressed and purified the GST-tagged eIF3 subunits from bacteria (Extended Data Fig. 4f) and tested them for binding to His–METTL3 using in vitro binding assays with either His–METTL3 or 1–200 a.a. METTL3 (and 1–200 a.a.) were found to specifically interact with eIF3h (Fig. 1e). The interaction between eIF3h with METTL3 was further confirmed using an anti-METTL3 antibody (that recognizes a 1–250 a.a. METTL3 epitope) to specifically disrupt this eIF3h–METTL3 interaction (Extended Data Fig. 4g). Additional GST pull-down experiments identified the MPN (Mpr1p and Pad1p N-terminal) domain[13] as necessary and sufficient to interact with METTL3 (Extended Data Fig. 4h–j). Notably, the MPN domain faces the solvent side of the ribosome and is probably accessible for interaction with METTL3 without impairing 80S assembly[13].

An in situ proximity ligation assay (PLA) confirmed METTL3–eIF3h proximity in cells (Fig. 1f). Co-immunoprecipitation experiments revealed that the association of METTL3 with translation initiation factors is dependent on eIF3h (Fig. 1g). We next tested the functional interaction between METTL3 and eIF3h, and found that depletion of eIF3h abrogated enhanced translation by METTL3 (Fig. 1h, Extended Data Fig. 4k–m). Overall, our results support a model whereby mRNA circularization and translation control is mediated by a specific METTL3–eIF3h interaction (Fig. 1i).

We next examined the widespread effect of METTL3 on mRNA translation (Fig. 2, Extended Data Fig. 5). METTL3 depletion caused an increase in the 80S ribosome peak and a corresponding reduction of polyribosome peak (Fig. 2a). METTL3 depletion had a negligible effect on steady-state mRNA abundance whereas translation efficiency of a large subset (4,267) of mRNAs was reduced by at least twofold in METTL3-depleted cells (Fig. 2b–d). Comparison of these genes with previously reported METTL3 photoactivatable ribonucleoside-enhanced crosslinking and immunoprecipitation (PAR-CLIP) data[14] identified 809 mRNAs that are both bound and translationally regulated by METTL3 (Fig. 2d). mRNAs on this list of METTL3 targets have on average longer 3′ UTRs compared to all mRNAs (Fig. 2e). Gene Ontology showed that these mRNAs are involved in tumour progression and apoptosis (Extended Data Fig. 5b). Quantitative PCR with reverse transcription (RT–qPCR) analysis confirmed that METTL3 depletion had a modest effect on mRNA abundance (Extended Data Fig. 5c), but strongly decreased translation of target mRNAs (Fig. 2f). Moreover, neither global mRNA stability analysis by RNA sequencing (RNA-seq) (Fig. 2g) nor RT–qPCR analysis of individual genes (Extended Data Fig. 5d, e) showed any differences in mRNA stability upon METTL3 depletion. We isolated endogenous METTL3 mRNPs and confirmed the association with target mRNAs by RT–qPCR (Fig. 2h, Extended Data Fig. 6a). Western blotting showed decreased protein expression from these target mRNAs in the METTL3-knockdown samples (Fig. 2i), whereas analysis of mRNA sequencing data revealed that the splicing patterns of these target mRNAs was unaltered (Extended Data Fig. 6b). Depletion of YTHDF1, a m$^6$A-reader protein implicated in translational control, had no effect on the expression of these METTL3 targets[7] (Extended Data Fig. 6c). Western blotting showed strongly reduced endogenous expression of bromodomain-containing protein 4 (BRD4) upon knockdown of eIF3h without affecting *BRD4* mRNA abundance or the levels of METTL3 protein (Fig. 2j, Extended Data Fig. 6d). Expression of a short-hairpin RNA (shRNA)-resistant Flag–METTL3 rescued the expression of BRD4 and CD9 proteins. However, expression of a catalytic mutant of METTL3 failed to recover target gene expression (Fig. 2k). METTL3 knockdown in A549 lung cancer cells similarly led to decreased expression of BRD4 and other targets (Fig. 2l), and treatment of METTL3-depleted

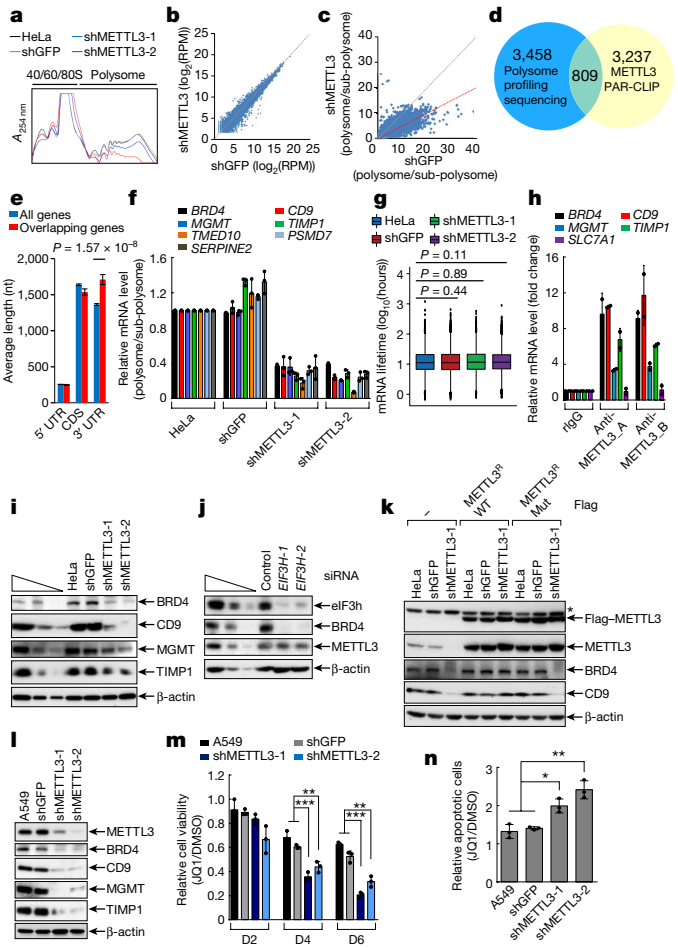


**Fig. 2 | METTL3 promotes translation of a large subset of mRNAs.** **a**, Polysome profile. Plot is representative of two independently performed experiments with similar results. **b**, Scatter plot of RNA-seq data. Average read number from two METTL3 knockdowns is plotted. As a control, shRNA targeting *GFP* (shGFP) was used. **c**, Scatter plot of translation efficiency. Average read number from two shMETTL3 samples were calculated by the ratio of polysome fraction to the read number in the sub-polysome fraction (40/60/80S) and plotted on the y-axis. **d**, Venn diagram showing mRNAs with a greater than twofold change in translation efficiency and with METTL3 PAR-CLIP data. **e**, Features of overlapping mRNAs ($n = 809$) from **d** was compared with all (18,115) expressed genes. Data are mean ± s.e.m. *P* values are from an unpaired two-sided *t*-test. **f**, RT–qPCR analysis. Data are mean ± s.d. from three technical replicates. **g**, Box plot represents stability profiling of global mRNA (12,479 mRNAs) from two biological replicates. *P* values are from a two-sided Wilcoxon rank sum test; the results are not statistically significant. **h**, RT–qPCR analysis of METTL3-associated mRNAs using two different anti-METTL3 antibodies (anti-METTL3_A and anti-METTL3_B). Data are mean ± s.d. from two independent experiments. **i–l**, Western blots. Cells were expressed with indicated shRNA, siRNA or plasmids. Blots are representative of at least two independently performed experiments with similar results. **m**, MTS assay of A549 cellular proliferation upon JQ1 treatment. **n**, Quantification of (sum of early and late) apoptotic cells. **m**, **n**, Data are mean ± s.d. from three independent experiments. *P* values are from a two-sided *t*-test with multiple comparison; $***P < 0.001$, $**P < 0.01$, $*P < 0.05$.

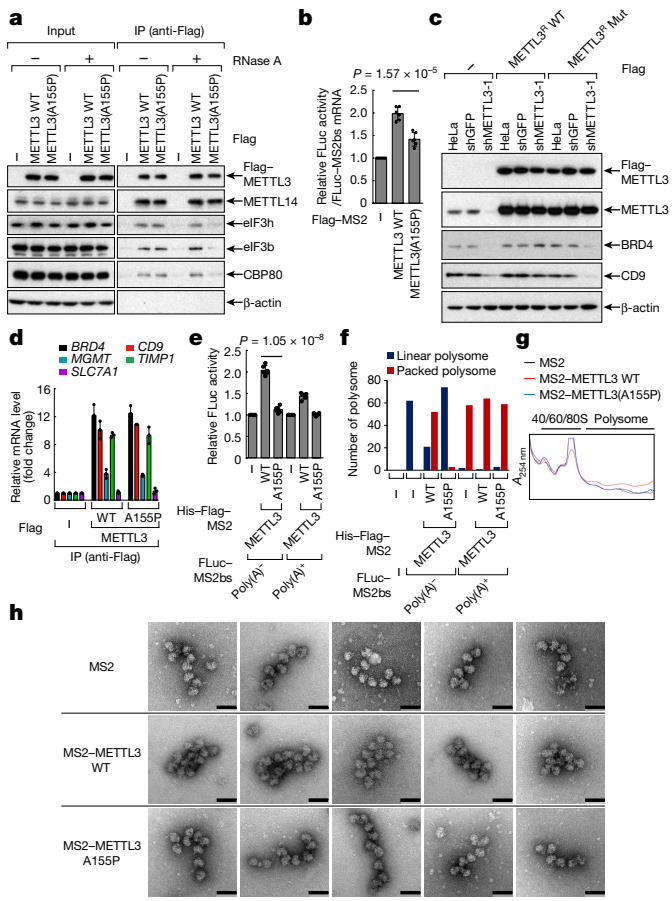


**Fig. 3 | METTL3–eIF3h interaction is crucial for enhanced mRNA translation and polysome conformation.** **a**, Co-immunoprecipitation of Flag–METTL3 or Flag–METTL3(A155P) analysed by western blotting using the indicated antibodies. Where indicated, lysates were treated with RNase A. Blots are representative of two independently performed experiments with similar results. **b**, Tethering assay to measure translation efficiency of reporter mRNAs. Data are mean ± s.d. from six independent experiments. *P* values are from a two-sided *t*-test. **c**, Western blot analysis using indicated antibodies. Two independently performed experiments show similar results. METTL3$^R$, cDNA containing nucleotide substitutions that make it resistant to shRNA for expression of wild-type or mutant METTL3 protein in the stable knockdown cells. **d**, RT–qPCR. Data are mean ± s.d. from two independent experiments. **e**, In vitro translation with rabbit reticulocyte lysate. Data are mean ± s.d. from six independent experiments. *P* values are from a two-sided *t*-test. **f**, Analysis of 20 images from each sample in **e**. **g**, Peak analysis of polysome profiling coupled with in vitro translation. Data are representative of two independently performed experiments with similar results. **h**, Electron microscopy images of polyribosomes. Images were taken from the samples in **g**. Scale bars, 50 nm. Images are representative of two independently performed experiments with similar results.

and control A549 cells with the BRD4 inhibitor JQ1 revealed that the METTL3-depleted cells are more sensitive to pharmacological BRD4 inhibition (Fig. 2m, n, Extended Data Fig. 6e).

Considering that 1–200 a.a. is sufficient to directly interact with eIF3h (Fig. 1 and Extended Data Fig. 4) and that 1–200 a.a. can promote translation in tethering experiments whereas 1–150 a.a. does not (Extended Data Fig. 2), we reasoned that a region between 150–200 a.a. must be important for the physical and functional METTL3–eIF3h interaction. Secondary structure predictions identified a putative alpha helix (150–161 a.a.) that is highly conserved in mammals[15,16] (Extended Data Fig. 7a, b). Moreover, 3D modelling identified a putative structured module[17] (Extended Data Fig. 7c). We therefore generated a mutant version of METTL3 with a single amino acid substitution of a highly conserved alanine (A155P) to disrupt this putative helical structure. Co-immunoprecipitation confirmed substantially impaired interaction of METTL3(A155P) with translation initiation factors, specifically in RNase-treated samples (Fig. 3a). Notably, the A155P mutation did not disrupt METTL3 interaction with METTL14 (Fig. 3a). Tethering experiments demonstrated that the METTL3(A155P) mutant is strongly impaired in promoting mRNA translation (Fig. 3b, Extended Data Fig. 7d, e). Moreover, expression of METTL3(A155P) in METTL3-depleted cells failed to rescue the expression of endogenous

target proteins (Fig. 3c). This effect was not due to altered mRNA association of METTL3(A155P) with endogenous target mRNAs (Fig. 3d and Extended Data Fig. 7f). In summary, although the METTL3 A155P mutant can associate with METTL14 and be loaded on mRNAs, its ability to interact with initiation factors and promote mRNA translation is severely compromised.

We next used in vitro-reconstituted translation assays to explore the effect of 3′ UTR-bound METTL3 on translation efficiency and polysome conformation (Fig. 3e, f, Extended Data Figs. 7g, 9a). Consistent with Extended Data Fig. 1g, tethering of recombinant METTL3 increased translation efficiency with a stronger effect on mRNA lacking a poly(A) tail (Fig. 3e). By contrast, tethered METTL3(A155P) had no significant effect on translation (Fig. 3e). Electron microscopy analysis of samples from the in vitro translation reactions showed mostly densely packed polysome structures formed when METTL3 was tethered to reporter mRNAs lacking a poly(A) tail (Extended Data Fig. 9a). By contrast, almost all the polysomes observed in the METTL3(A155P) sample appeared as linear polysomes (as in the control sample). Only dispersed ribosomes were observed in reactions without mRNA (Fig. 3f, Extended Data Fig. 9a). In all samples with mRNAs with poly(A) tails, mostly packed polysomes were observed irrespective of the protein that was tethered. As the reporter mRNA contains a very short 3′ UTR, it is expected that the known eIF4GI–PABP interaction is probably responsible for observed packed polysomes in poly(A)$^+$ samples (Fig. 3f, Extended Data Fig. 9a). We further analysed in vitro translation assays by sucrose gradient fractionation. Tethering of wild-type METTL3 resulted in a larger polysome peak compared to the METTL3(A155P) mutant (Fig. 3g). Individual polysomes were analysed using electron microscopy (Fig. 3g, h). Polysomes formed with wild-type METTL3 appeared to be more densely packed compared to the more linear polysomes that formed with the A155P mutant or MS2 control (Fig. 3h). Taken together, these results strongly support our model that METTL3 through its interaction with eIF3h promotes translation through its effects on polysome conformation.

Considering that METTL3 regulates the translation of a large subset of genes that are involved in tumour progression and apoptosis (Extended Data Fig. 5b), we examined the role of METTL3 in cancer. Immunohistochemistry staining of primary human lung adenocarcinoma samples and adjacent normal control tissue revealed that METTL3 expression is significantly increased in lung tumours and correlates with tumour stage (Fig. 4a, b, Extended Data Fig. 8a). METTL3 depletion in A549 lung cancer cells resulted in significantly smaller tumours in mouse xenografts (Fig. 4c, Extended Data Fig. 8b–d).

We next examined the relevance of the METTL3–eIF3h interaction and mRNA looping in the context of cancer-cell biology. Knockdown of eIF3h suppressed the ability of METTL3 to promote cellular invasion (Fig. 4d, Extended Data Fig. 8e). Moreover, unlike wild-type METTL3 protein, expression of either a catalytically inactive mutant or the METTL3(A155P) mutant was unable to promote the invasive capability of lung fibroblasts (Fig. 4e, Extended Data Fig. 8f). Furthermore, METTL3 overexpression was sufficient to promote the oncogenic transformation of NIH-3T3 cells, mouse embryonic fibroblasts (MEFs) or MB352 (p53-null MEFs) cells, whereas METTL3(A155P) had no significant effect in these 3D soft agar colony formation assays (Fig. 4f–h, Extended Data Fig. 8g, h). The oncogenic function of METTL3 was also studied in the mouse xenografts. NIH-3T3 cells with ectopic expression of wild-type METTL3, METTL3(A155P) or the empty-vector control were injected into nude mice to determine their in vivo tumorigenic capacities. Overexpression of wild-type METTL3 promoted in vivo tumour growth, whereas METTL3(A155P) showed an impaired ability to promote tumour growth. As control, no tumours were detected in mice injected with control NIH-3T3 cells (Fig. 4i, Extended Data Fig. 8i). Overall, these results support that the METTL3–eIF3h-mediated mRNA looping is critical for the oncogenic function of METTL3.

Methylated-RNA immunoprecipitation with sequencing (meRIP–seq) performed on four primary human lung tumours identified patient-specific and commonly m$^6$A-modified mRNAs in lung cancer

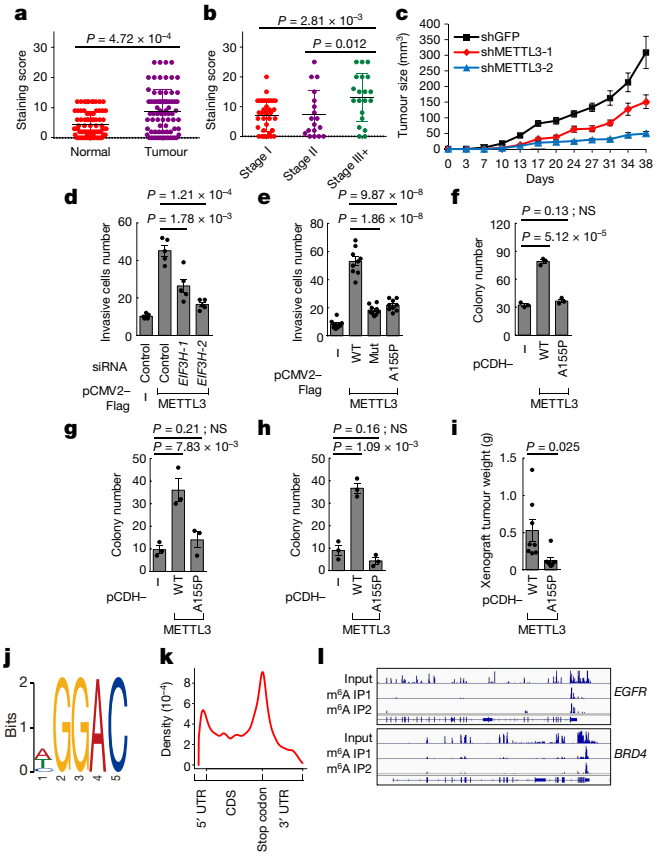


**Fig. 4 | Role of METTL3 and m$^6$A in lung cancer cells and primary human tumours. a**, **b**, Analysis of METTL3 immunohistochemical staining in primary lung adenocarcinoma and adjacent normal tissue. **a**, Normal tissue versus tumour tissue. Data are mean ± s.d. from 75 tissue samples. *P* value from a two-sided Wilcoxon signed-rank test. **b**, METTL3 levels in tumours of various stages. Data are mean ± s.d.; Stage I, $n = 37$; Stage II, $n = 18$; Stage III, $n = 20$. *P* values are from two-sided Wilcoxon signed-rank tests. **c**, Tumour growth of xenografts from A549 cells stably expressing indicated shRNAs. Data are mean ± s.e.m. from 5 mice. **d**, **e**, Quantification of invasive BJ cells. Cells were transiently transfected with indicated siRNAs (**d**) or plasmids (**e**). Data are mean ± s.e.m. from five (**d**) or nine (**e**) independent experiments. *P* values are from two-sided *t*-tests. **f**, Quantification of colony formation of NIH-3T3. **g**, **h**, Quantification of MEFs (**g**) or MB352 (**h**) colony formation. **f**–**h**, Data are mean ± s.e.m. from three independent experiments. *P* values from a two-sided *t*-test; NS, not significant. **i**, Tumour weight of xenografts derived from NIH-3T3 cells stably expressing the indicated proteins. There was no tumour formation in the empty vector group during the observed period. Data are mean ± s.e.m. from eight independent mice. *P* value is from a two-sided *t*-test. **j**–**l**, Global profiling of m$^6$A targets in primary lung cancer samples. **j**, Sequence motif identified in m$^6$A meRIP–seq. **k**, Metagene analysis of m$^6$A peaks. **l**, Integrative genomics viewer plots of representative m$^6$A-containing genes. Data is representative of four lung tumours with similar results.

(Extended Data Fig. 8j, Supplementary Table 3). An expected GGAC motif was identified and m$^6$A peaks are predominantly localized near the translation stop codon (Fig. 4j, k, Extended Data Fig. 8k). Gene Ontology analysis revealed that the common methylated genes are enriched in the signature genes of neoplasms and cancer, including the known oncogenes *EGFR* and *BRD4* (Fig. 4l, Extended Data Fig. 9b). These data were consistent with m$^6$A features identified in cell lines, with more than 50% of the peaks found in both tumours and cancer cell lines (Extended Data Fig. 9c).

We propose that METTL3 promotes oncogene translation and tumorigenesis through a mRNA looping mechanism. This is supported by: 1) the position-dependent effects of METTL3 tethering on mRNA translation; 2) electron-microscopy visualization of METTL3 bound

to endogenous polyribosomes and its proximity to cap-binding proteins; 3) METTL3 interaction with eIF3h and 4) the disruption of METTL3–eIF3h interaction abolishes the ability of METTL3 to promote translation, affect polysome conformation or promote oncogenic transformation. This METTL3–eIF3h loop presumably promotes translation through ribosome recycling in a way similar to that proposed for eIF4G–PABPC1-mediated mRNA looping. Although there is probably some redundancy between these mRNA circularization mechanisms, looping between the stop codon and the 5′ end might represent a more productive way to recycle ribosomes rather than via the 3′ end, especially for mRNAs with long 3′ UTRs as the ribosomes will dissociate from the mRNP once released at the stop codon.

The complexity of eIF3 and the specialized roles of individual subunits are only beginning to be appreciated[18,19]. Imbalanced expression of eIF3 subunits is found in various tumours[20] and expression in fibroblasts can promote malignant transformation[21]. Increased eIF3h expression is found in different tumour types and in many cases is due to amplification of a chromosomal region that includes *EIF3H* at 8q23.3 and the nearby *MYC* oncogene[22,23]. METTL3 is overexpressed in many different types of cancer (Extended Data Fig. 10a), and the expression of METTL3 and eIF3h is often positively correlated (Extended Data Fig. 10b, c). Our findings could pave the way for the development of new cancer therapeutic strategies.

## Online content

Any methods, additional references, Nature Research reporting summaries, source data, statements of data availability and associated accession codes are available at https://doi.org/10.1038/s41586-018-0538-8.

Received: 7 July 2017; Accepted: 14 August 2018;
Published online 19 September 2018.

1. Lin, S., Choe, J., Du, P., Triboulet, R. & Gregory, R. I. The m$^6$A methyltransferase METTL3 promotes translation in human cancer cells. *Mol. Cell* **62**, 335–345 (2016).
2. Barbieri, I. et al. Promoter-bound METTL3 maintains myeloid leukaemia by m$^6$A-dependent translation control. *Nature* **552**, 126–131 (2017).
3. Vu, L. P. et al. The $N^6$-methyladenosine (m$^6$A)-forming enzyme METTL3 controls myeloid differentiation of normal hematopoietic and leukemia cells. *Nat. Med.* **23**, 1369–1376 (2017).
4. Chen, M. et al. RNA $N^6$-methyladenosine methyltransferase METTL3 promotes liver cancer progression through YTHDF2 dependent post-transcriptional silencing of SOCS2. *Hepatology* **67**, 2254–2270 (2017).
5. Meyer, K. D. & Jaffrey, S. R. The dynamic epitranscriptome: $N^6$-methyladenosine and gene expression control. *Nat. Rev. Mol. Cell Biol.* **15**, 313–326 (2014).
6. Wang, X. et al. $N^6$-methyladenosine-dependent regulation of messenger RNA stability. *Nature* **505**, 117–120 (2013).
7. Wang, X. et al. $N^6$-methyladenosine modulates messenger RNA translation efficiency. *Cell* **161**, 1388–1399 (2015).
8. Xu, C. et al. Structural basis for selective binding of m$^6$A RNA by the YTHDC1 YTH domain. *Nat. Chem. Biol.* **10**, 927–929 (2014).
9. Imataka, H., Gradi, A. & Sonenberg, N. A newly identified N-terminal amino acid sequence of human eIF4G binds poly(A)-binding protein and functions in poly(A)-dependent translation. *EMBO J.* **17**, 7480–7489 (1998).
10. Wells, S. E., Hillner, P. E., Vale, R. D. & Sachs, A. B. Circularization of mRNA by eukaryotic translation initiation factors. *Mol. Cell* **2**, 135–140 (1998).
11. Borman, A. M., Michel, Y. M., Malnou, C. E. & Kean, K. M. Free poly(A) stimulates capped mRNA translation *in vitro* through the eIF4G-poly(A)-binding protein interaction. *J. Biol. Chem.* **277**, 36818–36824 (2002).
12. Tarun, S. Z., Jr. & Sachs, A. B. Association of the yeast poly(A) tail binding protein with translation initiation factor eIF-4G. *EMBO J.* **15**, 7168–7177 (1996).
13. des Georges, A. et al. Structure of mammalian eIF3 in the context of the 43S preinitiation complex. *Nature* **525**, 491–495 (2015).
14. Liu, J. et al. A METTL3–METTL14 complex mediates mammalian nuclear RNA $N^6$-adenosine methylation. *Nat. Chem. Biol.* **10**, 93–95 (2014).
15. Ashkenazy, H. et al. ConSurf 2016: an improved methodology to estimate and visualize evolutionary conservation in macromolecules. *Nucleic Acids Res.* **44**, W344–W350 (2016).
16. Kouza, M., Faraggi, E., Kolinski, A. & Kloczkowski, A. The GOR method of protein secondary structure prediction and its application as a protein aggregation prediction tool. *Methods Mol. Biol.* **1484**, 7–24 (2017).
17. Kelley, L. A., Mezulis, S., Yates, C. M., Wass, M. N. & Sternberg, M. J. The Phyre2 web portal for protein modeling, prediction and analysis. *Nat. Protocols* **10**, 845–858 (2015).
18. Lee, A. S., Kranzusch, P. J. & Cate, J. H. eIF3 targets cell-proliferation messenger RNAs for translational activation or repression. *Nature* **522**, 111–114 (2015).
19. Lee, A. S., Kranzusch, P. J., Doudna, J. A. & Cate, J. H. eIF3d is an mRNA cap-binding protein that is required for specialized translation initiation. *Nature* **536**, 96–99 (2016).
20. Hershey, J. W. The role of eIF3 and its individual subunits in cancer. *Biochim. Biophys. Acta* **1849**, 792–800 (2015).
21. Zhang, L., Pan, X. & Hershey, J. W. Individual overexpression of five subunits of human translation initiation factor eIF3 promotes malignant transformation of immortal fibroblast cells. *J. Biol. Chem.* **282**, 5790–5800 (2007).
22. Mahmood, S. F. et al. A siRNA screen identifies *RAD21*, *EIF3H*, *CHRAC1* and *TANC2* as driver genes within the 8q23, 8q24.3 and 17q23 amplicons in breast cancer with effects on cell growth, survival and transformation. *Carcinogenesis* **35**, 670–682 (2014).
23. Zhang, L., Smit-McBride, Z., Pan, X., Rheinhardt, J. & Hershey, J. W. An oncogenic role for the phosphorylated h-subunit of human translation initiation factor eIF3. *J. Biol. Chem.* **283**, 24047–24060 (2008).

**Acknowledgements** Thanks to Y. K. Kim for CBP80 and CTIF antibodies. S.L. was supported by a Damon Runyon-Sohn Pediatric Fellowship (DRSG-7–13) and a grant from Alex's Lemonade Stand Foundation. R.I.G. was supported by grants from the US National Institute of General Medical Sciences (NIGMS) (R01GM086386) and National Cancer Institute (NCI) (R01CA211328).

**Reviewer information** *Nature* thanks C. Mason and the other anonymous reviewer(s) for their contribution to the peer review of this work.

**Author contributions** J.C., S.L. and R.I.G. designed the research; J.C., S.L., W.Z., L.W., J.R.-M. and W.K. performed all the experiments; J.C. performed in vitro translation assay, tethering assay, polysome fractionation and RNA-seq, co-immunoprecipitation, electron microscopy, cap-association assay and in situ PLA; S.L. performed GST pull-down assay, far-western blotting, immunohistochemical staining, cell invasion assay and m$^6$A meRIP–seq; W.Z. performed soft agar colony formation assays and in vivo tumour xenograft; L.W. performed electron microscopy; J.R.-M. performed cell proliferation and apoptosis assays; W.K. performed in situ PLA; S.L., Q.L., P.D. and S.T. performed all bioinformatics analysis; W.G.R. and K.-K.W. provided human lung cancer patient samples; N.L. provided eIF3 complex. P.Sl., P.Sa., R.E.G. and F.J.S. contributed to discussion. J.C., S.L. and R.I.G. analysed data and wrote the paper with input from other authors.

**Competing interests** The authors declare no competing interests.

**Additional information**
**Extended data** is available for this paper at https://doi.org/10.1038/s41586-018-0538-8.
**Supplementary information** is available for this paper at https://doi.org/10.1038/s41586-018-0538-8.
**Reprints and permissions information** is available at http://www.nature.com/reprints.
**Correspondence and requests for materials** should be addressed to R.I.G.
**Publisher's note:** Springer Nature remains neutral with regard to jurisdictional claims in published maps and institutional affiliations.

## METHODS

**Cell culture and transfection.** Human lung cancer cell lines (A549 and H1299), HEK293T, BJ, NIH-3T3, HeLa cells and MEFs were cultured with DMEM supplemented with 10% fetal bovine serum (FBS) and antibiotics. Cells were grown in a 5% $CO_2$ cell culture incubator at 37 °C. Cell lines were authenticated using morphology-, karyotyping- and PCR-based approaches by ATCC. The cell lines were tested for potential mycoplasma contamination and confirmed that they are mycoplasma negative. Transfection of plasmids was performed using Lipofectamine 2000 (Invitrogen) according to the manufacturer's instructions. Down regulation of target genes by siRNA was performed using Lipofectamine RNAi Max (Invitrogen). The following siRNA sequences were used in this study: 5′-r(GAUAGAUGGCCUUGUGGUA)(UU)-3′ for eIF3h-1; 5′-r(GCGGAGCCU UCGCCAUGUA)(UU)-3′ for eIF3h-2; 5′-r(UGAGAAAGGAGGAGAGGAA) d(TT)-3′ for eIF4GI; 5′-r(UCAACCUCUUUACGGAUUU)d(TT)-3′ for eIF3b; and 5′-r(GCAUCAACCUGAAUGACAU)(UU)-3′ for CTIF.

**Virus production and generation of stable knockdown and overexpression cells.** Virus-mediated generation of stable knockdown and overexpression cells were performed as previously described[1]. In brief, shRNA containing pLKO.1 vector was co-transfected with pLP1, pLP2, and VSVG into 293T cells. For overexpression, pCDH vectors containing the wild-type *METTL3* (*METTL3* WT) and A155P cDNA were co-transfected with Delta 8.9 and VSVG plasmids into 293T cells. Viruses were collected at 48 h and 72 h after transfection and then used to infect cells with Polybrene (8 mg/ml, Sigma); 48 h after infection, puromycin was added to the culture medium to select the infected cells.

**Plasmid construction.** pFLAG-METTL3 WT, pFLAG-MS2-METTL3 and pFLAG-MS2-METTL3 Mut, have previously been described[1]. pFLAG-METTL3 A155P plasmids were generated by inducing point mutation in pFLAG-METTL3 WT using Q5 Site-Directed Mutagenesis Kit (NEB E0554). Plasmids pFLAG-MS2-METTL3 (1–100), pFLAG-MS2-METTL3 (1–150), pFLAG-MS2-METTL3 (1–200), pFLAG-MS2-METTL3 (1–350) and pFLAG-MS2-METTL3 (101–580) was constructed by substitution of PCR-amplified each METTL3 fragment into the NotI–*METTL3* WT–BglII site of pFLAG-MS2-METTL3. For stable METTL3 overexpression, wild-type *METTL3* and A155P sequence were PCR-amplified and cloned into the NheI and NotI sites of pCDH-CMV-MCS-EF1-Puro plasmid. For expression of recombinant METTL3 proteins, cDNA corresponding to full-length METTL3 and N-terminal amino acids 1–200 were cloned into the pETDuet-1 and pET His6 GST TEV LIC cloning vector individually. For expression of recombinant METTL3 proteins for in vitro translation, Flag–MS2, Flag–MS2–METTL3 (1–200), Flag–MS2–METTL3, Flag–MS2–METTL3(A155P) were cloned into pETDuet-1. For bacteria protein expression of human eIF3h, eIF3j and eIF3m that express N-terminal GST-fused proteins, BamHI/EcoRI fragment of pGEX2TK vector was ligated to the PCR amplified BamHI/EcoRI fragment that contained eIF3h, eIF3j or eIF3m. In addition, for the pGEX2TK-eIF3g or -eIF3i, BglII/EcoRI fragment of pGEX2TK vector was ligated to the PCR amplified BglII/EcoRI fragment that contained either eIF3g or eIF3i, respectively. For bacteria expression of eIF3h, deletion mutants were generated by ligation of BamHI/EcoRI fragment of pGEX2TK vector with BamHI/EcoRI fragment of either PCR-amplified eIF3h (1–222) or eIF3h (29–222). The pGL3c_TK luciferase reporter (FLuc) and pGL3c_TK luciferase reporter containing 2× MS2 binding sites near the stop codon (FLuc-MS2bs) have previously been described[1]. The 2× MS2 binding site sequence was PCR-amplified from FLuc-MS2bs and inserted into the NcoI site of pGL3c_TK luciferase reporter to make the FLuc-5′ UTR-MS2bs reporter that the MS2 binding sites are located in the 5′ UTR region of the luciferase gene. The 2× MS2 binding site sequence and GFP sequence (from CAG-GFP, Addgene Plasmid #16664) were cloned into the XbaI site of pGL3c_TK luciferase reporter (FLuc) to make the FLuc-MS2bs-GFP and FLuc-GFP-MS2bs reporters. For pFLAG-tethering effector plasmids, *METTL3* shRNA resistance plasmids were generated by introducing synonymous mutations into the shRNA targeting sequence using the Q5 Site-Directed Mutagenesis Kit (NEB E0554). All cloning primers are listed in Supplementary Table 1.

**In vitro translation assay.** H1299 cells were collected and resuspended in hypotonic buffer (10 mM Hepes (pH 7.4), 10 mM potassium acetate, 1.5 mM magnesium acetate, and 2.5 mM dithiothreitol (DTT)). Cells were then incubated on ice for 30 min and ruptured by passing ten times through a 25-gauge needle attached to a 3-ml syringe. The cell homogenate was centrifuged at 13,000*g* for 15 min at 4 °C. The supernatant was collected and used for in vitro translation. In vitro translation reactions were performed for 1 h at 30 °C using either H1299 cytoplasmic cell extracts or rabbit reticulocyte lysate (RRL) (Thermo FisherScientific, AM1200) in 20-μl reaction mixtures containing 100 ng of in vitro transcribed reporter mRNAs and 500 ng of either purified recombinant His–Flag–MS2, His–Flag–MS2–METTL3 or His–Flag–MS2–METTL3 (1–200) protein. The activity of in vitro-translated luciferase was measured using a Luciferase assay kit (Promega, E1960) according to the manufacturer's instructions. Reporter mRNAs either presence or absence of poly(A) tails were in vitro transcribed using PCR-amplified FLuc-MS2bs fragment with following primers; 5′-GACTAGTAATACGACTCACTATAGGG GCCACCATGGAAGACGCCAAAAACATAAAG-3′ (sense) and 5′-TCTAGA CCCCGGGAGCATGGGTGAT-3′ (antisense) for the FLuc-MS2bs Poly(A)$^-$ mRNA, and 5′-GACTAGTAATACGACTCACTATAGGGGCCACCATGGA AGACGCCAAAAACATAAAG-3′ (sense) and 5′-TTTTTTTTTTTTTTTTTTTT TTTTTTTTTTTCTAGACCCCGGGAGCATGGGTGAT-3′ (antisense) for the FLuc-MS2bs Poly(A)$^+$ mRNAs.

**RNA isolation and RT–qPCR.** The details of RNA isolation and RT–qPCR assays are as previously described[1]. In brief, RNA was extracted from cells, co-immunoprecipitation or sucrose gradient fractionation samples using Trizol (Invitrogen) according to the manufacturer's instructions. RT–qPCR analyses were performed using SYBR Green PCR Master Mix with the Step One Real-Time PCR System (AppliedBiosystems). All primers used in this study are listed in Supplementary Table 2. For the analysis of global or individual mRNA lifetime, METTL3-depleted or control HeLa cells (60-mm culture dishes) were treated with actinomycin D (5 μg/ml), then collected after 0 h, 2 h, 4 h and 6 h.

**Luciferase assay and translation efficiency.** Dual luciferase assays were performed according to the manufacturer's protocol (Promega). FLuc activity was normalized to the Renilla luciferase (RLuc) activity. Relative FLuc activity was normalized to the relative FLuc mRNAs. The normalized FLuc activity (translation efficiency) in the presence of Flag–MS2 was set to 1.

**Polysome fractionation and RNA-seq.** METTL3-depleted or control HeLa cells (four 150-mm culture dishes) were treated with 100 μg/ml cycloheximide (Sigma) for 10 min at 37 °C. Cells were then lysed and layered onto 10–50% sucrose gradient tube and centrifuged at 36,000 r.p.m. in a Beckman SW-41Ti rotor for 2.5 h at 4 °C. Gradients were fractionated and monitored at absorbance 254 nm (Brandel). Collected fractions were pulled into sub-polysome fraction and polysome fraction. Then, total RNA, sub-polysome and polysome samples were subjected to RNA-seq. Poly(A)-selected mRNAs were purified and used for library construction using TruSeq Stranded mRNA Sample Prep Kits (Illumina RS-122-2101) and sequenced with Illumina NextSeq 500. ERCC RNA Spike-In Control Mixes (Ambion) were added into each sample before constructing the library to normalize the reads.

**Co-immunoprecipitation, mass spectrometry and western blot.** Co-immunoprecipitation and western blot were performed as previously described[1]. In brief, Flag–METTL3-expressing HeLa or H1299 cells were collected and lysed using NET-2 buffer (50 mM Tris-HCl (pH 7.4), 150 mM NaCl, 1 mM phenylmethanesulfonylfluoride (PMSF), 2 mM benzamidine, 1% NP-40) then the supernatant was subjected to immunoprecipitation using anti-Flag M2 Affinity Gel (Sigma-Aldrich). Where indicated, the affinity elute was subjected to SDS–PAGE and then either colloidal Coomassie blue staining or western blotting. Bands were excised and subjected to mass spectrometric sequencing as previously described[1]. The following antibodies were used for western blotting: METTL3 (Proteintech, 15073-1-AP; Abcam, ab195352), β-actin (Abcam, ab8227), eIF3h (Abcam, ab60942) CBP80 (gift from Y. K. Kim, Korea University), CTIF (gift from Y. K. Kim, Korea University), eIF4E (Cell Signaling Technology, #2067), eIF3b (Santa Cruz Biotechnology, sc-16377), eIF4GI (Cell Signaling Technology, #2498), Flag (Sigma, A8592), BRD4 (Abcam, ab128874), CD9 (Cell Signaling Technology, #13174), MGMT (Cell Signaling Technology, #2739), TIMP1 (Cell Signaling Technology, #8946) and FTO (Phosphosolution, 597-FTO).

**Protein expression, purification and GST pull-down assay.** Plasmids expressing the recombinant proteins were transformed into BL21 *Escherichia coli* and then the recombinant proteins were induced by IPTG at 20 °C overnight. The bacteria were pelleted and resuspended in protease inhibitor containing PBST buffer and then lysed by sonication. His-tag recombinant proteins were purified using Ni-NTA agarose (Qiagen 30210). The GST-tagged proteins were purified using the glutathione sepharose (BioVision 6655) according to the manufacturer's protocol. For GST pull down assay, equal amount of GST fusion proteins or GST control bound to glutathione sepharose were incubated with purified recombinant His-tagged full-length METTL3 or N-terminal (1–200) fragment for 1 h at 4 °C, after extensive washing, the proteins bound to the sepharose were resolved on SDS–polyacrylamide gels and detected by western blot analysis.

**Far-western blotting.** Far-western blotting was performed with biochemically purified human eIF3 protein complex that was resolved by SDS–PAGE and then transferred to Hybond ECL nitrocellulose membrane. The membrane was first incubated in blocking buffer (100 mM Tris (pH 7.5), 100 mM potassium acetate, 2 mM magnesium acetate, 0.1 mM EDTA, 10% glycerol, 1 mM PMSF, 1 mM benzamidine, and 0.05% Tween 20, 5% non-fat milk) at 4 °C overnight, then the membrane was incubated with blocking buffer containing 5 μg of purified recombinant full-length METTL3 or METTL3 (1–200) proteins at 4 °C for another 24 h. After that, the membrane was incubated with METTL3 antibody for western blotting analysis.

**Electron microscopy.** Flag–METTL3 expressing H1299 cells were collected and lysed using NET-2 buffer, then the supernatant was subjected to immunoprecipitation using anti-Flag M2 Affinity Gel (Sigma-Aldrich). Resin-bound mRNP complexes were eluted using 3×Flag peptides (Sigma, F3290). Where indicated, during the elution, anti-METTL3 antibody (Proteintech, 15073-1-AP) and gold nanoparticle

(6 nm) conjugated anti-rabbit IgG were added with or without either anti-CBP80 antibody or anti-eIF4E antibody that was gold-nanoparticle (10 nm)-conjugated using GOLD conjugation kit (Abcam, ab201808), according to the manufacturer's instructions. The eluates were then fractionated using 10–50% sucrose gradients. Each fraction was applied to an electron-microscopy grid (EMS, G400-Cu) covered with a thin layer of carbon and after 1 min the excess suspension was blotted with a filter paper. The grid was washed twice with water and 0.7% uranyl formate, and then negatively stained for 20 s with 0.7% uranyl formate. The specimens were examined in Tecnai G2 Spirit BioTWIN Transmission Electron Microscope (FEI company) with AMT 2k CCD camera equipped. Direct magnification of 68,000× was used to detect images from Extended Data Fig. 9a, and magnification of 98,000× was used to detect images from Figs. 1b, 3h and Extended Data Fig. 4a, c. Polysome numbers were counted using 20 individual pictures for each sample with direct magnification of 30,000× in Fig. 3f. All the images shown in the figures are cropped sections. The average distance between immuno-gold particles in Extended Data Fig. 4d was measured from the images in Fig. 1b and Extended Data Fig. 4c using the electron microscope software (AMT Capture engine). In vitro translation reactions were performed for 1 h at 30 °C using RRL, and then the total reaction mixture was subjected to illustra MicroSpin S-400 HR Columns (Fig. 3f, Extended Data Fig. 9a) or sucrose gradient fractionation (Fig. 3g, h). The eluates were then applied to an electron-microscopy grid and analysed by electron microscopy.

**Cap-association assay using m$^7$GTP-agarose.** To analyse the interaction of METTL3 and the cap-binding protein complex, cells were lysed using NET2 buffer and total cell extracts were incubated with m$^7$GTP-agarose (Jena Bioscience, AC-155S) for 2 h at 4 °C. Then, the beads were washed five times and suspended in SDS sample buffer. The eluted samples were analysed by western blot. Where indicated, 75 μM of m$^7$G(5′)ppp(5′)G Cap Analogue (Ambion, AM8048) was added into the sample and incubated with m$^7$GTP-agarose.

**Cell proliferation, apoptosis and invasion assays.** Cell proliferation, apoptosis and invasion assays were performed as described[1]. In brief, for cell proliferation, 700 cells were seeded in a 96-well plate on day 0 with the pertinent treatment. JQ1 (500 nM) was used. Absorbances at 490 nm were measured using CellTiter 96 AQueous One Solution Cell Proliferation Assay kit (Promega) on day 2, day 4, and day 6 to measure the cellular proliferation. The numbers of apoptotic cells were quantified by flow cytometric assays using Annexin V-FITC Apoptosis Detection Kit (BioVision) five days after 500 nM of JQ1 treatment and cell seeding. Cell invasion was measured using BioCoat Matrigel Invasion Chamber (Corning) according to the manufacturer's instructions.

**Soft agar colony formation assays.** NIH-3T3, MEFs and MB352 cells at 30% confluence were infected with the lentivirus expressing indicated protein for 48 h in the presence of 8 μg/ml polybrene (Sigma). Two days after infection, puromycin was added to the medium at 2.5 μg/ml, and cells were selected for 1 week. Fifty thousand live NIH-3T3 cells, 100,000 live MEFs or 100,000 live MB352 (p53 null MEFs) cells were selected and mixed with 0.35% top-agar and were plated onto 0.6% base-agar in six-well plates. Twenty-five days (NIH-3T3) or thirty days (MEFS or MB352) after plating the cells into soft agar, colony numbers were counted. The colony numbers were counted by openCFU.

**PLA.** HeLa cells were incubated with primary antibodies (rabbit anti-METTL3 antibody and mouse anti-eIF3h antibody) in blocking solution at 4 °C for 2 h. Cells were then washed for five times for 5 min in PBS plus 0.1% Tween 20. Then, cells were incubated with secondary proximity probes (anti-Rabbit-PLUS and anti-Mouse-MINUS) (Sigma, DUO92101) for 90 min at 37 °C. Cells were washed five times for 5 min in 10 mM Tris-HCl (pH 7.5) plus 0.1% Tween 20 at 37 °C, then twice for 5 min in PBS plus 0.1% Tween 20. All subsequent steps were performed according to the manufacturer's instruction. Cells were observed with a Zeiss LSM 710 Multiphoton Laser Scanning Confocal.

**Immunohistochemistry staining.** The human lung cancer tumour array was purchased from Biomax (HLug-Ade150CS-01). The slide was baked for 60 min in an oven set to 60 °C and then loaded into the Bond III staining platform with appropriate labels. Antigen was retrieved by Bond Epitope Retrieval 2 for 20 min. Then the slide was incubated with METLL3 antibody (Abcam, ab195352) at 1:500 for 30 min at room temperature. Primary antibody was detected using Bond Polymer Refine Detection kit. Slides were developed in DAB, then dehydrated and coverslipped. Each sample was scored by the percentage of positively stained cells (percentage score: 1–5) and the staining intensity (intensity score: 1–5). Then the sample staining score was calculated by multiplying the percentage score and the intensity score.

**In vivo tumour xenograft.** All research involving animals complied with protocols approved by the Beth Israel Deaconess Medical Center Institutional Animal Care and Use Committee. Four-to-six-week-old female NU/J (Nude) immunodeficient mice (Jackson Laboratory #002019) were used for subcutaneous injections. Randomly divided five mice (A549 cells) or eight mice (NIH-3T3 cells) were used for each group. One hundred thousand A549 cells or 1,500,000 NIH-3T3 cells in serum-free medium and growth-factor-reduced Matrigel (Corning #354230) (1:1) were inoculated into the flank of nude mice. The xenograft tumour formation was monitored using callipers twice a week. The recipient mice were monitored and euthanized when the tumours reached 1-cm diameter. The tumour volume was calculated by use of a formula 1/2(length × width2). The investigator was blinded to group allocation.

**m$^6$A meRIP–seq and data analysis.** meRIP–seq was performed as previously described[1]. All the studies involving human patient samples complied with protocols approved by the Institutional Review Board. Informed consent was obtained from all participants. Portions of fresh tumour tissue approximately 0.5 × 0.5 × 0.5 cm were snap-frozen and preserved at −80 °C, pulverized in liquid nitrogen and stabilized in Trizol for total RNA isolation. Then, the mRNA purification from total RNA was performed using PolyATtract mRNA Isolation Systems (Promega). Two micrograms of the purified mRNA was fragmented and immunoprecipitated with anti-m$^6$A antibody (Synaptic Systems, 202003). The purified RNA fragments from m$^6$A MeRIP were used for library construction using the TruSeq Stranded mRNA Sample Prep Kits (Illumina RS-122-2101) and sequenced with Illumina NextSeq 500. Reads mapping, peak calling, metagene analysis and motif search were performed as previously described[1]. To identify the alternative splicing events, all the clean RNA-seq reads of control and METTL3 knockdown samples were first trimmed to the same length (72 bp), which were then aligned against the human hg19 (GRCh37) reference genome using Tophat2[24]. rMATS v.3.2.5[25] was used to detect the splicing events and significant splicing differences between METTL3 knockdown and control samples. To analyse the global profiling of mRNA lifetime, the clean reads were aligned to human reference genome (hg19) using Tophat2[24] after trimming the adapters and filtering low-quality sequences from the raw data. The reads mapped to each gene were counted using HTSeq[26] on the basis of the GENCODE gene model (v19)[27]. The raw counts were then normalized as reads per kilobase per million mapped reads. ERCC RNA Spike-In Control Mixes (Ambion) were added into each sample before constructing the library to normalize the reads. mRNA lifetime was calculated according to the method in the previous study[8]. To analyse METTL3 or eIF3h expression level among tumours from the Cancer Genome Analysis (TCGA), RNA-seq data for 33 TCGA tumour types were downloaded from Genomic Data Commons Data Portal (GDC) of TCGA (https://cancergenome.nih.gov/) using R package TCGAbiolinks[28] The expression matrix was then constructed by merging the transcripts per million values of all downloaded RNA-seq samples. The tumour types without corresponding normal tissue samples were excluded and the retained 24 tumour types with normal tissues were used to draw the box plot of gene expression. *P* values are calculated by Wilcoxon rank-sum test, with asterisks indicating statistical significance.

**Statistics and reproducibility.** Data are presented as the mean ± s.e.m. or mean ± s.d. Statistical significance was determined by a Student's two-tailed *t*-test for RT–qPCRs and Luciferase assays. Where applicable, Shapiro–Wilk test and Q–Q plotting (quantile–quantile plot) were performed before Student's two-tailed *t*-test to assess whether the data plausibly came from a normal distribution. Where indicated, Shapiro–Wilk signed-rank test was used. $P < 0.05$ was considered statistically significant. Sample size for Extended Data Fig. 10a, b; $n = 408$, $n = 1{,}095$, $n = 304$, $n = 36$, $n = 285$, $n = 184$, $n = 155$, $n = 520$, $n = 66$, $n = 533$, $n = 290$, $n = 371$, $n = 515$, $n = 501$, $n = 178$, $n = 179$, $n = 497$, $n = 94$, $n = 259$, $n = 103$, $n = 415$, $n = 505$, $n = 120$ and $n = 176$, from the order of left to right for primary solid tumour; $n = 19$, $n = 133$, $n = 3$, $n = 9$, $n = 41$, $n = 11$, $n = 5$, $n = 44$, $n = 25$, $n = 72$, $n = 32$, $n = 50$, $n = 59$, $n = 51$, $n = 4$, $n = 3$, $n = 52$, $n = 10$, $n = 2$, $n = 1$, $n = 35$, $n = 59$, $n = 2$ and $n = 24$, from the order of left to right for normal tissue. Sample size for Extended Data Fig. 10c; $n = 285$, $n = 184$, $n = 155$, $n = 371$, $n = 515$, $n = 501$, $n = 497$ and $n = 94$, from the order of left to right.

**Code availability.** Script and code used for data analysis can be found at https://github.com/rnabioinfor/rnamethy.

**Reporting summary.** Further information on experimental design is available in the Nature Research Reporting Summary linked to this paper.

## Data availability

The m$^6$A meRIP–seq and RNA-seq data have been deposited in the Gene Expression Omnibus (GEO) under accession number GSE117299. All other data are available from the authors on request.


24. Kim, D. et al. TopHat2: accurate alignment of transcriptomes in the presence of insertions, deletions and gene fusions. *Genome Biol.* **14**, R36 (2013).
25. Shen, S. et al. rMATS: robust and flexible detection of differential alternative splicing from replicate RNA-Seq data. *Proc. Natl Acad. Sci. USA* **111**, E5593–E5601 (2014).
26. Harrow, J. et al. GENCODE: the reference human genome annotation for The ENCODE Project. *Genome Res.* **22**, 1760–1774 (2012).
27. Anders, S., Pyl, P. T. & Huber, W. HTSeq—a Python framework to work with high-throughput sequencing data. *Bioinformatics* **31**, 166–169 (2015).
28. Colaprico, A. et al. TCGAbiolinks: an R/Bioconductor package for integrative analysis of TCGA data. *Nucleic Acids Res.* **44**, e71 (2016).

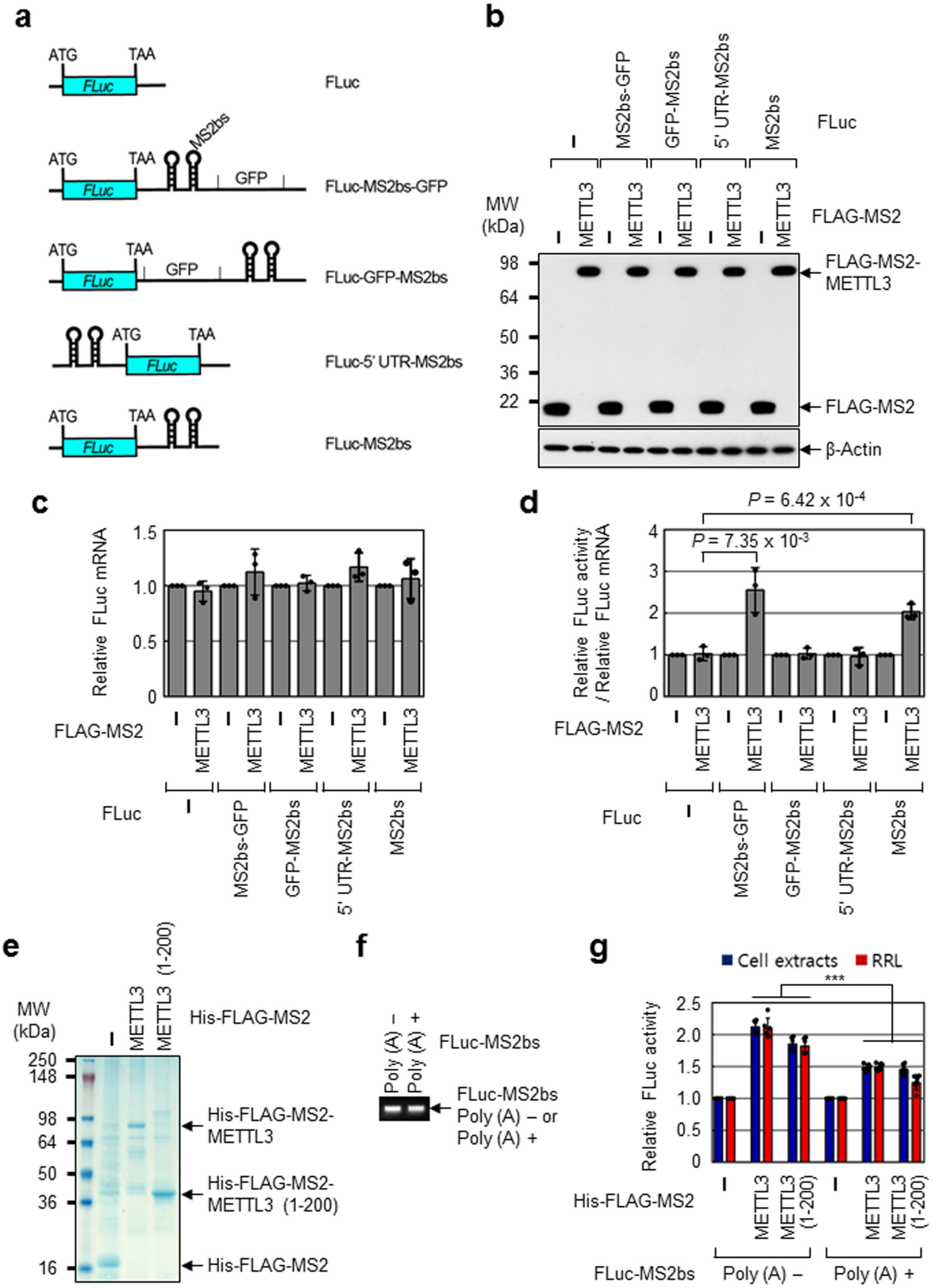


**Extended Data Fig. 1** | See next page for caption.

**Extended Data Fig. 1 | METTL3 binding close to the stop codon enhances translation. a**, Schematic of reporter plasmids containing Firefly luciferase cDNA and different positions of MS2 binding sites. **b**, Western blotting with indicated antibodies. Blot is representative of two independently performed experiments with similar results. **c**, RT–qPCR analysis of reporter mRNAs. Each tested reporter mRNAs were normalized to RLuc mRNAs. The FLuc:RLuc ratio for each construct with Flag–MS2 expression was set to 1. Data are mean ± s.d. from three biologically independent samples. **d**, Tethering assay to measure translation efficiency as described in Fig. 1h. Data are mean ± s.d. from three biologically independent samples. *P* values from a two-sided *t*-test. **e**, Colloidal Coomassie blue staining of recombinant protein His–Flag–MS2, His–Flag–MS2–METTL3, or His–Flag–MS2–METTL3 (1–200). **f**, Ethidium bromide-stained agarose gel electrophoresis of the indicated in vitro transcribed reporter mRNAs; FLuc-MS2bs without poly (A) tail (Poly (A) -) or FLuc-MS2bs with 30-nt poly (A) tail (Poly (A) +). **f**, **g**, Images are representative of two independently performed experiments with similar results. **g**, In vitro translation of reporter mRNAs using either H1299 cell extracts or rabbit reticulocyte lysate (RRL). The levels of in vitro-translated FLuc protein were analysed using luciferase assays. Value of FLuc activity in the presence of His–Flag–MS2 recombinant protein was set to 1. Data are mean ± s.d. from six independent experiments. *P* value is from a two-sided *t*-test; $***P < 0.001$, multiple comparison.

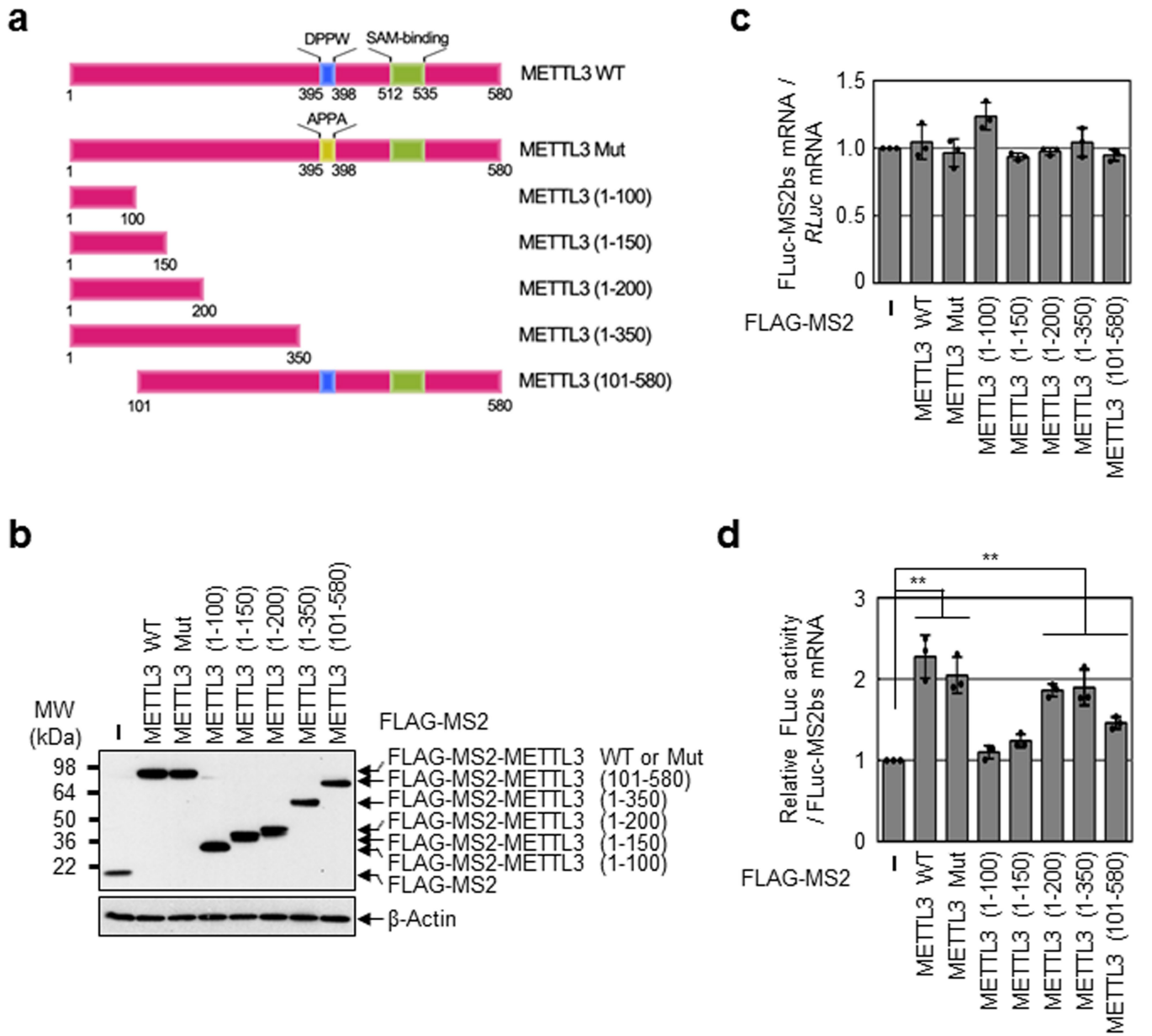


**Extended Data Fig. 2 | N-terminal region of METTL3 promotes translation. a**, Schematic of METTL3-deletion mutants or mutation in METTL3 catalytic domain. **b**, Western blotting with indicated antibodies. The blot is representative of two independently performed experiments with similar results. **c**, RT–qPCR analysis of reporter mRNAs. FLuc–MS2bs mRNA levels were normalized to RLuc mRNAs. The FLuc:RLuc ratio obtained in Flag–MS2 (control) was set to 1. Data are mean ± s.d. from three biologically independent samples. **d**, Tethering assay to measure translation efficiency of reporter mRNAs as described in Fig. 1h. Data are mean ± s.d. from three biologically independent samples. *P* value is from a two-sided *t*-test; $^{**}P < 0.01$, multiple comparison.

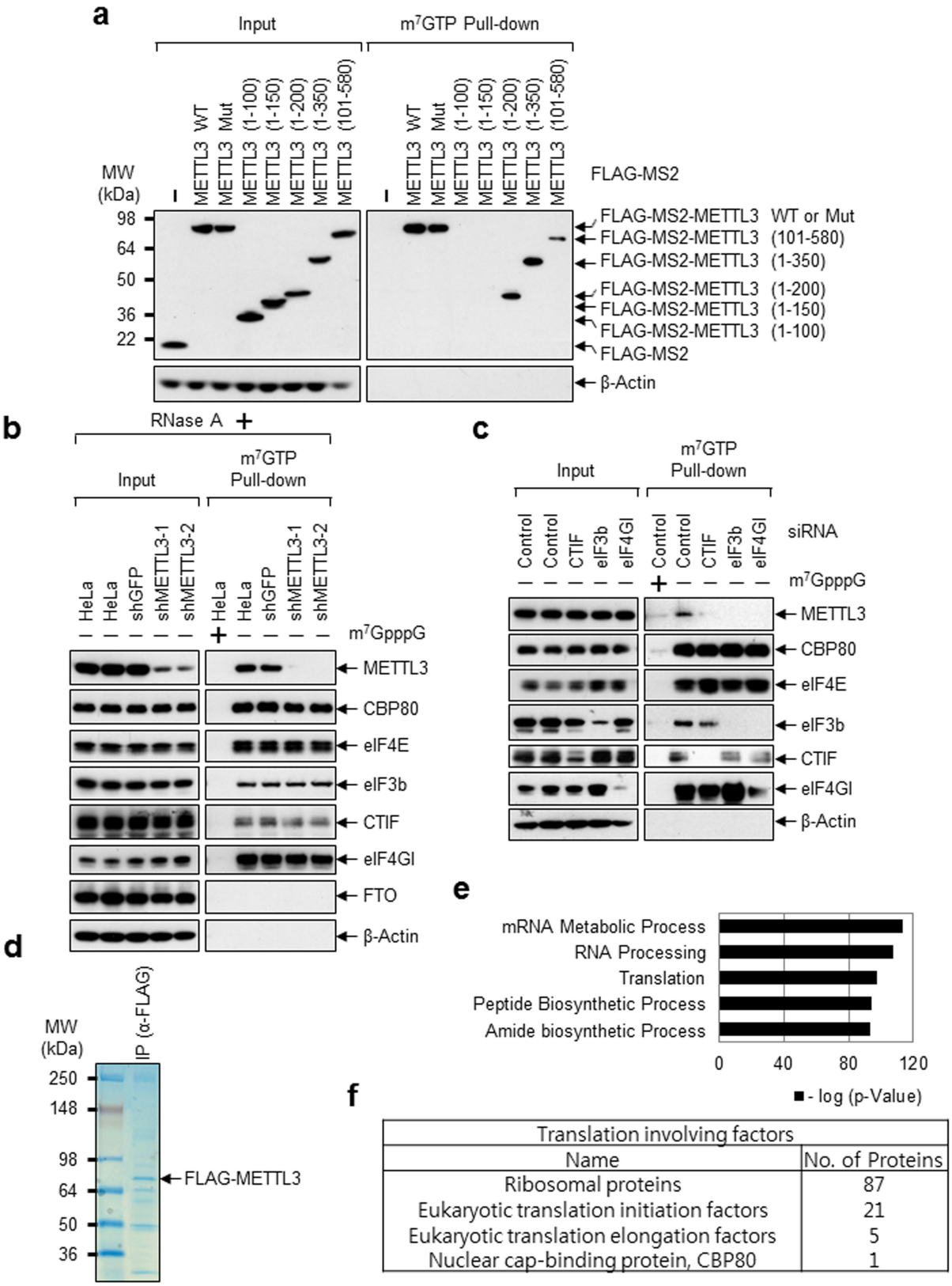


f

| Translation involving factors | |
|---|---|
| Name | No. of Proteins |
| Ribosomal proteins | 87 |
| Eukaryotic translation initiation factors | 21 |
| Eukaryotic translation elongation factors | 5 |
| Nuclear cap-binding protein, CBP80 | 1 |

**Extended Data Fig. 3** | See next page for caption.

**Extended Data Fig. 3 | METTL3 associates with translation initiation factors. a**, Deletion mutants of METTL3 were expressed in HeLa cell. The total-cell extracts (Input) and the cap-associated protein samples were analysed by western blotting using the indicated antibodies. **b**, Cap-association assay with METTL3 depletion. The total-cell extracts (Input) and the cap-bound protein samples were analysed by western blotting using the indicated antibodies. $m^7$GpppG cap analogue was used for antagonizing cap-associating proteins binding to $m^7$GTP-agarose. **c**, Same as **b**, except HeLa cells were transfected with *CTIF*, *EIF3B* or *EIF4G1* siRNA. In **a**, **b**, blots are representative of two independently performed experiments with similar results. **d–f**, Mass spectrometry of Flag–METTL3 interacting proteins. **d**, Proteins that were co-immunopurified with Flag–METTL3 subjected to 4–12% Tris–glycine SDS–PAGE. Colloidal Coomassie blue staining was performed. **e**, Gene Ontology analysis of the identified proteins from mass spectrometry. One experiment was performed. Hypergeometric distribution (one-tail) with Bonferroni adjustment was used to determine enrichment statistical significance. **f**, Table showing the translation involving factors identified from mass spectrometry.

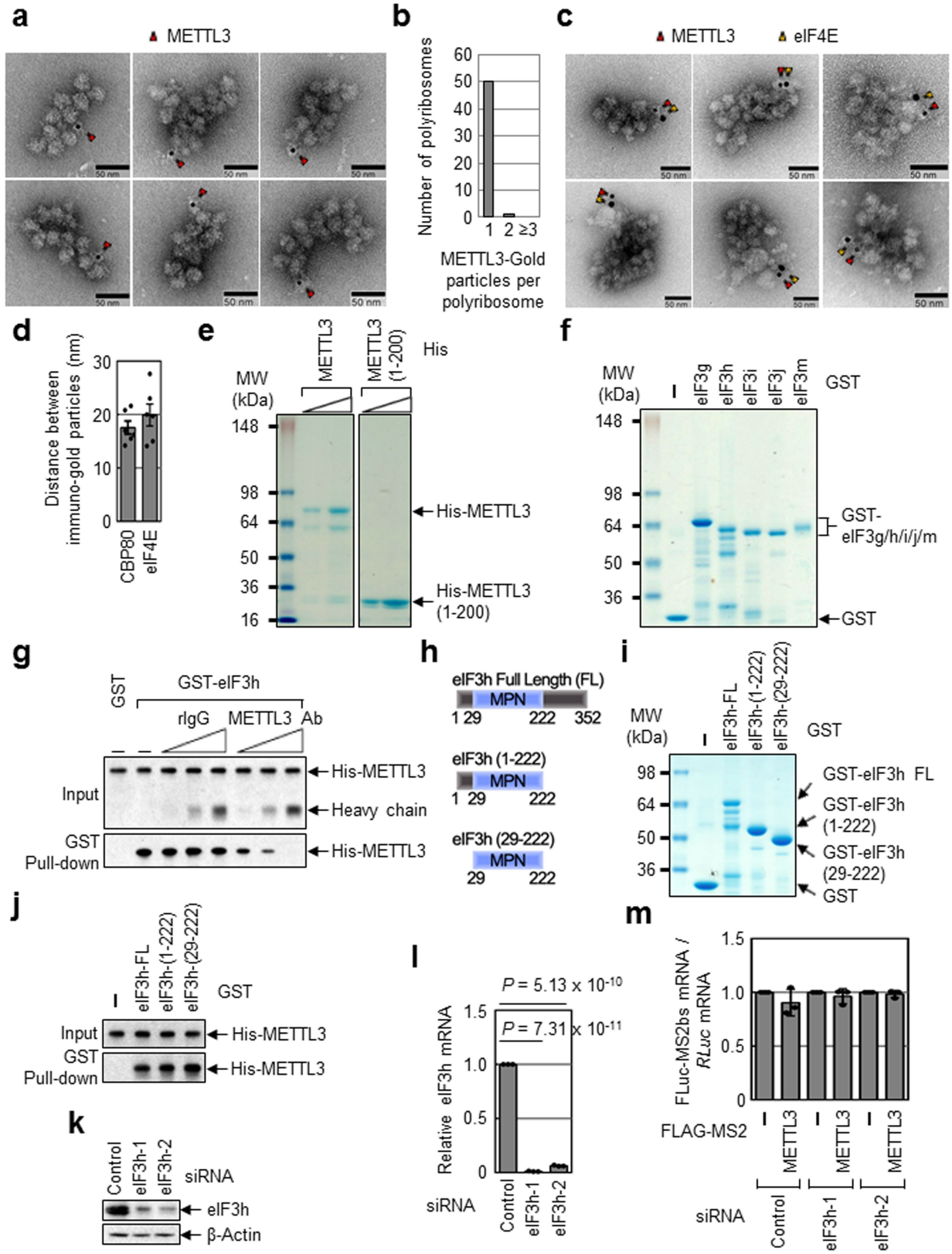


**Extended Data Fig. 4** | See next page for caption.

**Extended Data Fig. 4 | N-terminal region of METTL3 directly interacts with MPN domain of eIF3h. a**, Electron-microscopy images of polyribosome with gold-particle labelling of METTL3. Red arrows indicate METTL3 with immuno-gold particle (6 nm). Images are representative of three independent experiments with similar results. **b**, Counting of METTL3 with gold-particle labelling in each polyribosome. **c**, Electron-microscopy images of polyribosome with METTL3 and eIF4E. Red arrows indicate METTL3 with immuno-gold particle (6 nm) and yellow arrows indicate eIF4E with immuno-gold particle (10 nm). Images are representative of four independently performed experiments with similar results. **d**, Mean distance between immuno-gold particles was measured. Data are mean ± s.d. of six biologically independent samples from at least three independent experiments. **e**, Colloidal Coomassie blue staining of recombinant protein His–METTL3 or His–METTL3 1–200 amino acid fragments. **f**, Colloidal Coomassie blue staining of recombinant GST-tagged protein eIF3g, eIF3h, eIF3i, eIF3j or eIF3m. **g**, GST–eIF3h was co-purified with His–METTL3 in the presence of either rabbit IgG (rIgG) or anti-METTL3 antibody. Levels of co-purified His–METTL3 were analysed by western blotting. **e**–**g**, Images are representative of two independently performed experiments with similar results. **h**, Schematic diagram of human eIF3h deletion mutants. **i**, Colloidal Coomassie blue staining of recombinant GST–eIF3h, GST–eIF3h (1–222) or GST–eIF3h (29–222). **j**, GST pull-down of the indicated eIF3h deletion mutants. Co-purified His–METTL3 was analysed by western blotting. **i**, **j**, One experiment was performed. **k**, Western blotting demonstrates efficient knockdown of eIF3h protein. Blots are representative of three independently performed experiments with similar results. **l**, RT–qPCR analysis demonstrates efficient down regulation of eIF3h mRNA. Data are mean ± s.d. from three biologically independent samples. *P* values are from a two-sided *t*-test. **m**, RT–qPCR analysis of reporter mRNAs. FLuc–MS2bs reporter mRNAs were normalized to RLuc mRNAs. The FLuc:RLuc ratio obtained in Flag–MS2 was set to 1. Data are mean ± s.d. from three biologically independent samples.

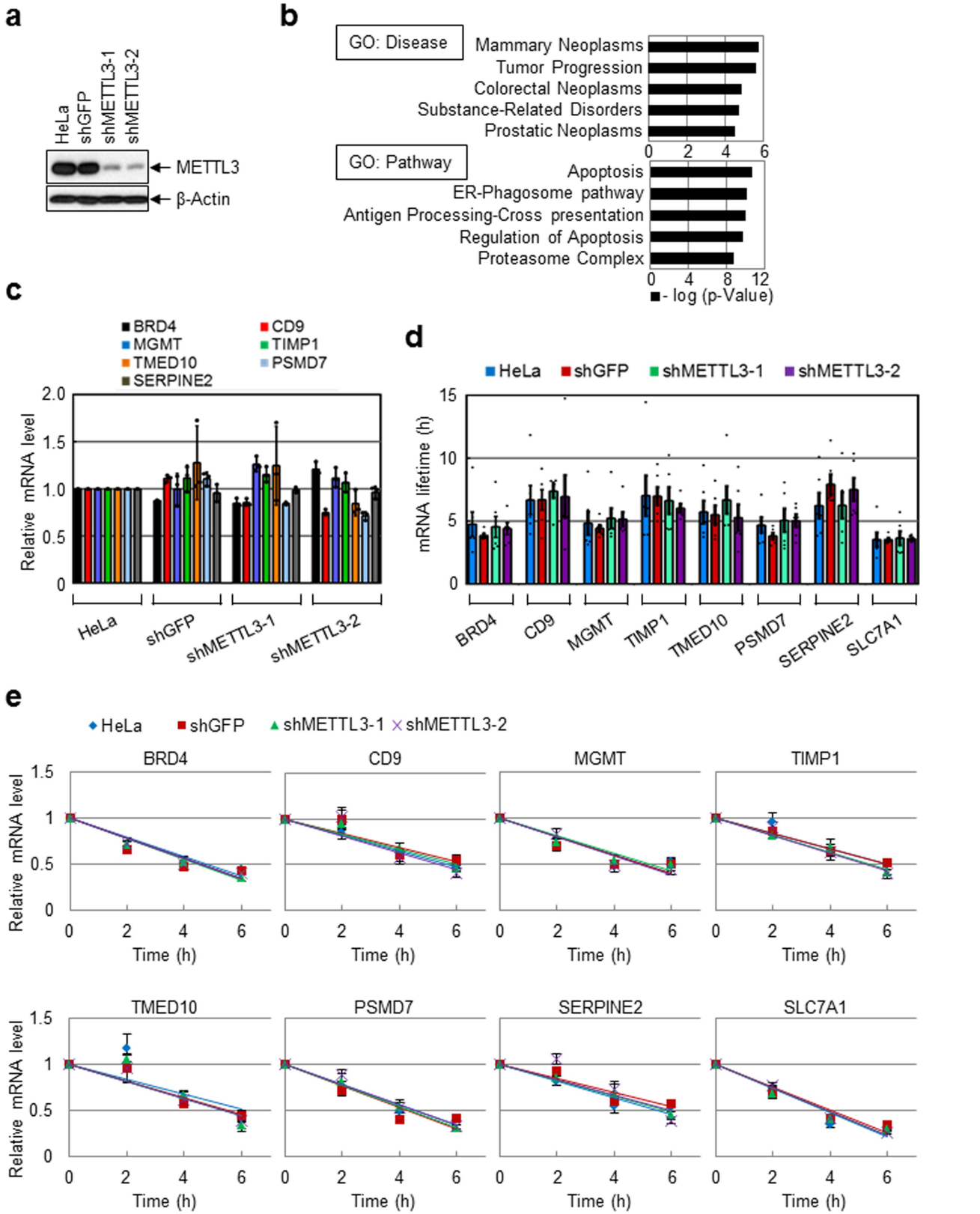


**Extended Data Fig. 5 | METTL3 has no significant effect on mRNA stability. a**, Western blotting with indicated antibodies. Blot is representative of three independently performed experiments with similar results. **b**, Gene Ontology analysis of the overlapping mRNAs ($n = 809$) in Fig. 2d. Hypergeometric distribution (one-tail) with Bonferroni adjustment was used to determine statistical significance of enrichment. **c**, RT–qPCR analysis using indicated primers. Data are mean ± s.d. from three technical replicates. **d**, **e**, Half-life of endogenous mRNAs was analysed by RT–qPCR using indicated primers. Data are mean ± s.e.m. from six independent experiments. **d**, *P* values are from a two-sided *t*-test; multiple comparison for the *P* values showed that there were no significant differences between the samples for all the tested mRNAs ($P > 0.05$).

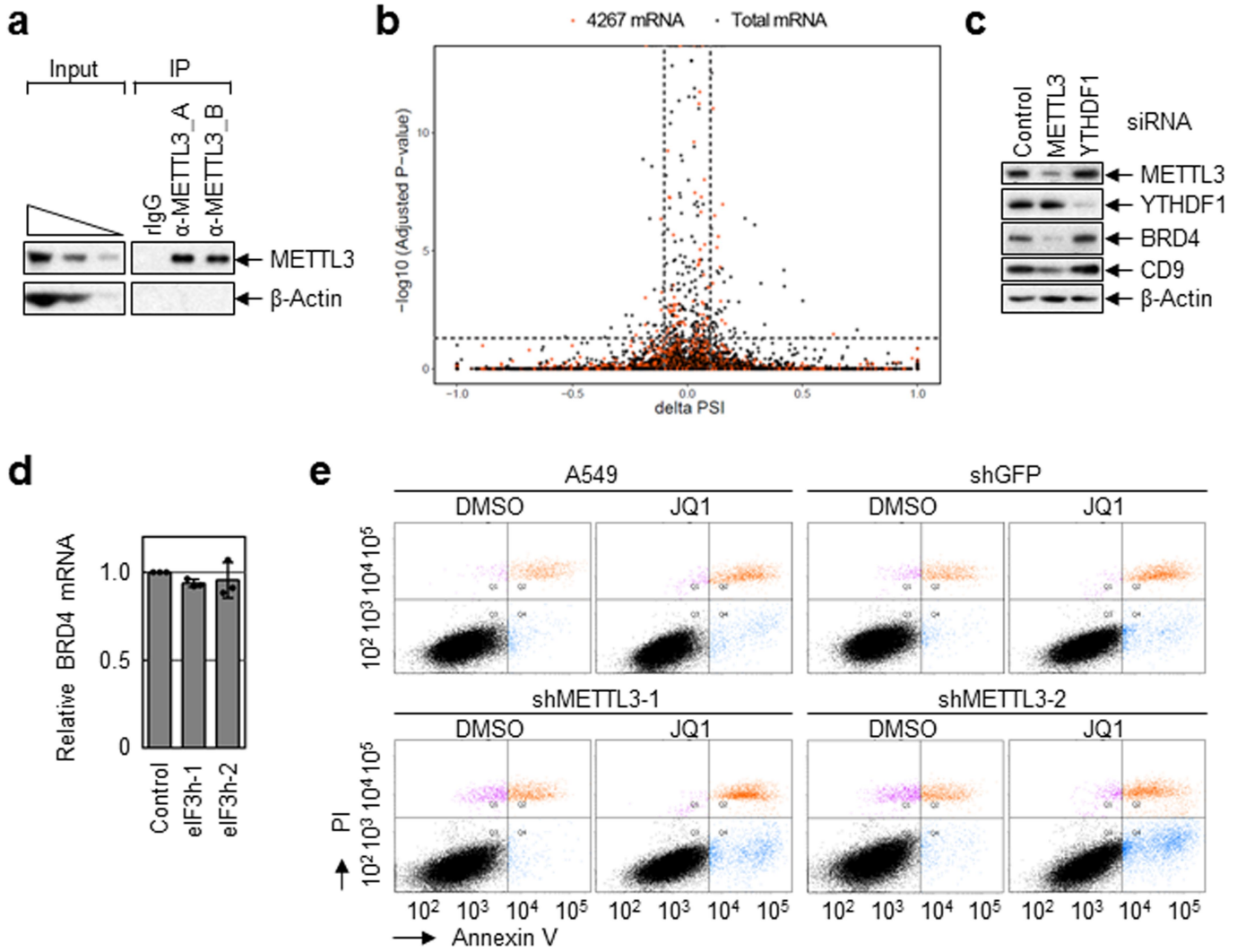


**Extended Data Fig. 6 | Widespread role of METTL3 in oncogene translation. a**, Immunoprecipitation of endogenous METTL3 and western blotting using the indicated antibodies. The blot is representative of two independently performed experiments with similar results. **b**, Density plot reflects the distribution of changes in percentage spliced in ΔPSI values and corresponding *P* values for alternative splicing events detected by rMATs v.3.2.5 (rMATs is developed on the basis of a hierarchical framework and likelihood-ratio test was used to detect differential splicing). Splicing events at a FDR < 5% and ΔPSI > 0.1 are considered as significant. Black dots indicate total mRNAs. Red dots (4,276 mRNAs) indicate mRNAs in METTL3-depleted cells that are translated more than twofold less. **c**, Western blot using indicated antibodies in control-, METTL3- or YTHDF1-knockdown cells. Blots are representative of two independently performed experiments with similar results. **d**, RT–qPCR analysis of endogenous *BRD4* mRNAs. Data are mean ± s.e.m. from three biologically independent samples. **e**, Annexin V/PI staining of METTL3 knockdown and control A549 cells upon JQ1 treatment (analysed by FACS). Data are from three independent experiments.

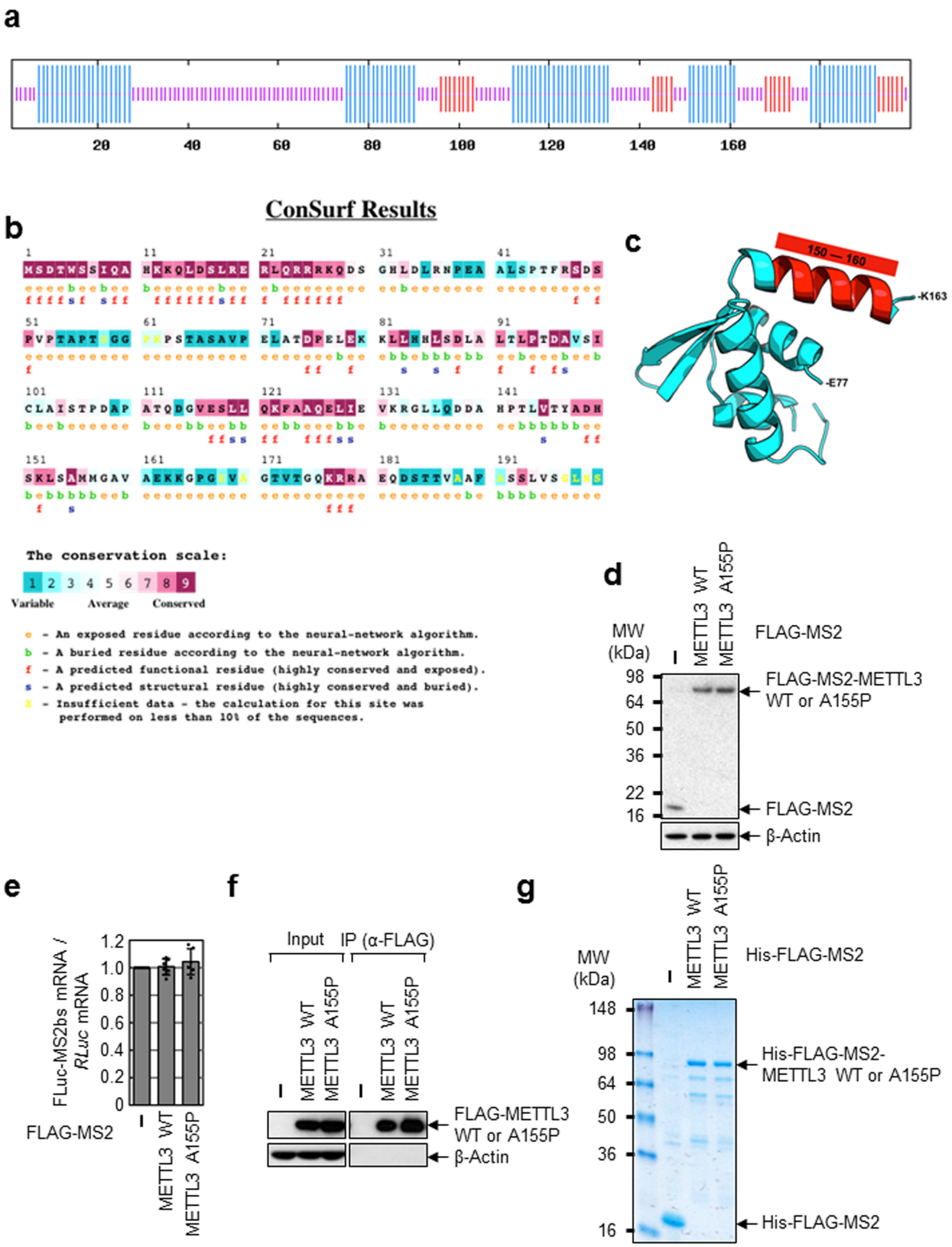


**Extended Data Fig. 7** | See next page for caption.

**Extended Data Fig. 7 | Identification of a conserved alanine residue in the N-terminal region of METTL3 required for its interaction with eIF3h. a**, Secondary structure prediction of the N-terminal (1–200) region of METTL3 protein showing putative alpha helices (blue lines). **b**, Evolutionary conservation of the N-terminal (1–200) region METTL3 protein. **c**, Computational modelling of the 3D structure of the N-terminal (77–163) region METTL3 protein, on the basis of the coordinates of RCSB Protein Data Bank entry 3HHH. **d**, Western blotting using the indicated antibodies. The blot is representative of two independently performed experiments with similar results. **e**, RT–qPCR analysis of reporter mRNAs. FLuc–MS2bs mRNA levels were normalized to RLuc mRNAs. The FLuc:RLuc ratio obtained in Flag–MS2 (control) was set to 1. Data are mean ± s.d. from six independent experiments. **f**, Immunoprecipitation of Flag–METTL3 (wild-type or METTL3(A155P)) and western blotting analysis using the indicated antibodies. Blots are representative of two independently performed experiments with similar results. **g**, Staining of recombinant protein wild-type His–Flag–MS2–METTL3 or His–Flag–MS2–METTL3(A155P). Gel is representative of two independently performed experiments with similar results.

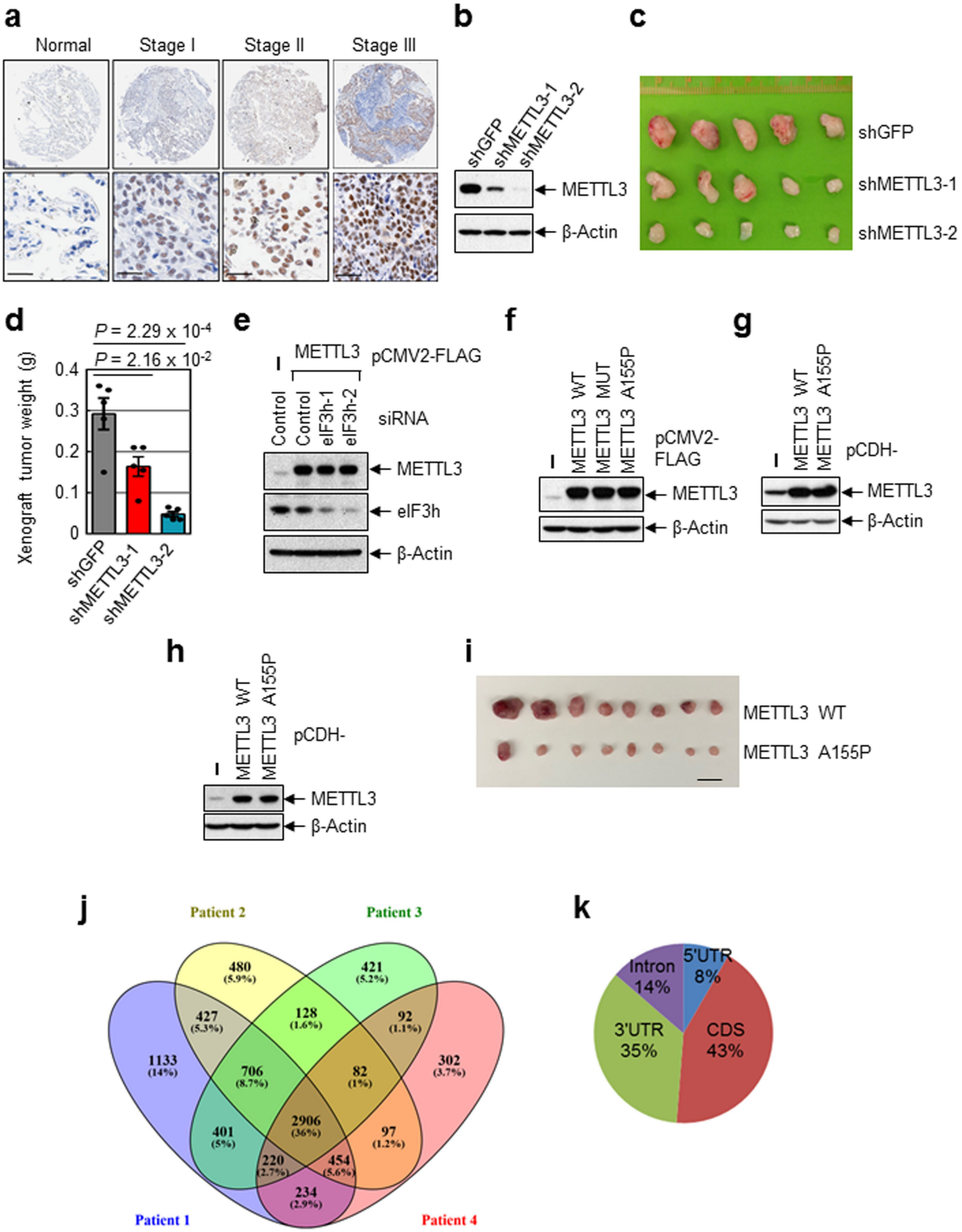


**Extended Data Fig. 8 | METTL3 expression correlates with lung tumour stage and promotes tumorigenicity. a**, Staining image of control and different stages lung cancer samples ($n = 75$). Bottom panels show the enlarged sections of the top panels. Scale bar, 30 μM. **b**, Western-blotting analysis using indicated antibodies. One experiment was performed. **c**, **d**, Tumour images (**c**) and plot of tumour weight (**d**) at the end point of the xenograft experiment. Data are mean ± s.e.m. from five independent mice. *P* values from a two-sided *t*-test. **e**–**h**, Western blotting analysis using the indicated antibodies. For **e**, two independently were performed experiments with similar results. For **f**–**h**, one experiment was performed. **i**, Tumour images at the endpoint in the xenograft experiment. Scale bar, 20 mm. **j**, Overlapping of genes containing $m^6A$ identified in four samples from patients with lung cancer. **k**, Distribution of $m^6A$ sites.

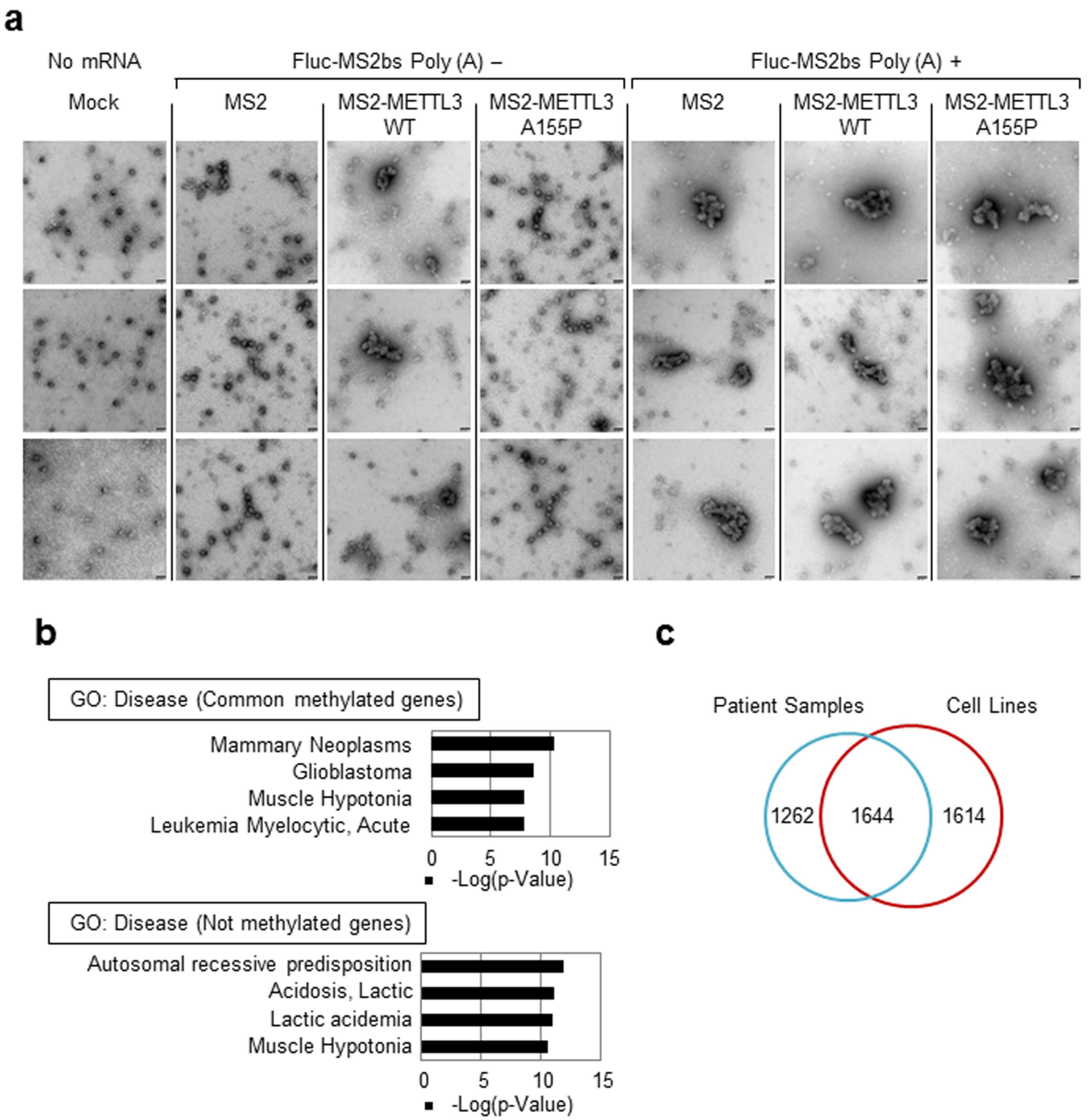


**Extended Data Fig. 9 | Polysome conformation is affected by METTL3 and m$^6$A modification in primary human lung tumours. a**, Electron-microscopy images of polyribosomes. Images were taken from the samples in Fig. 3e. Scale bar, 50 nm. Six independently performed experiments show similar results. **b**, Gene Ontology analysis. Common methylated genes refers to the methylated genes in all four patient samples. 'Not methylated genes' indicates genes that are not methylated in any of the four patient samples. Hypergeometric distribution (one-tail) with Bonferroni adjustment was used to determine enrichment statistical significance. **c**, Venn diagram showing m$^6$A peak overlap between patient tumour samples and cells (H1299 and A549).

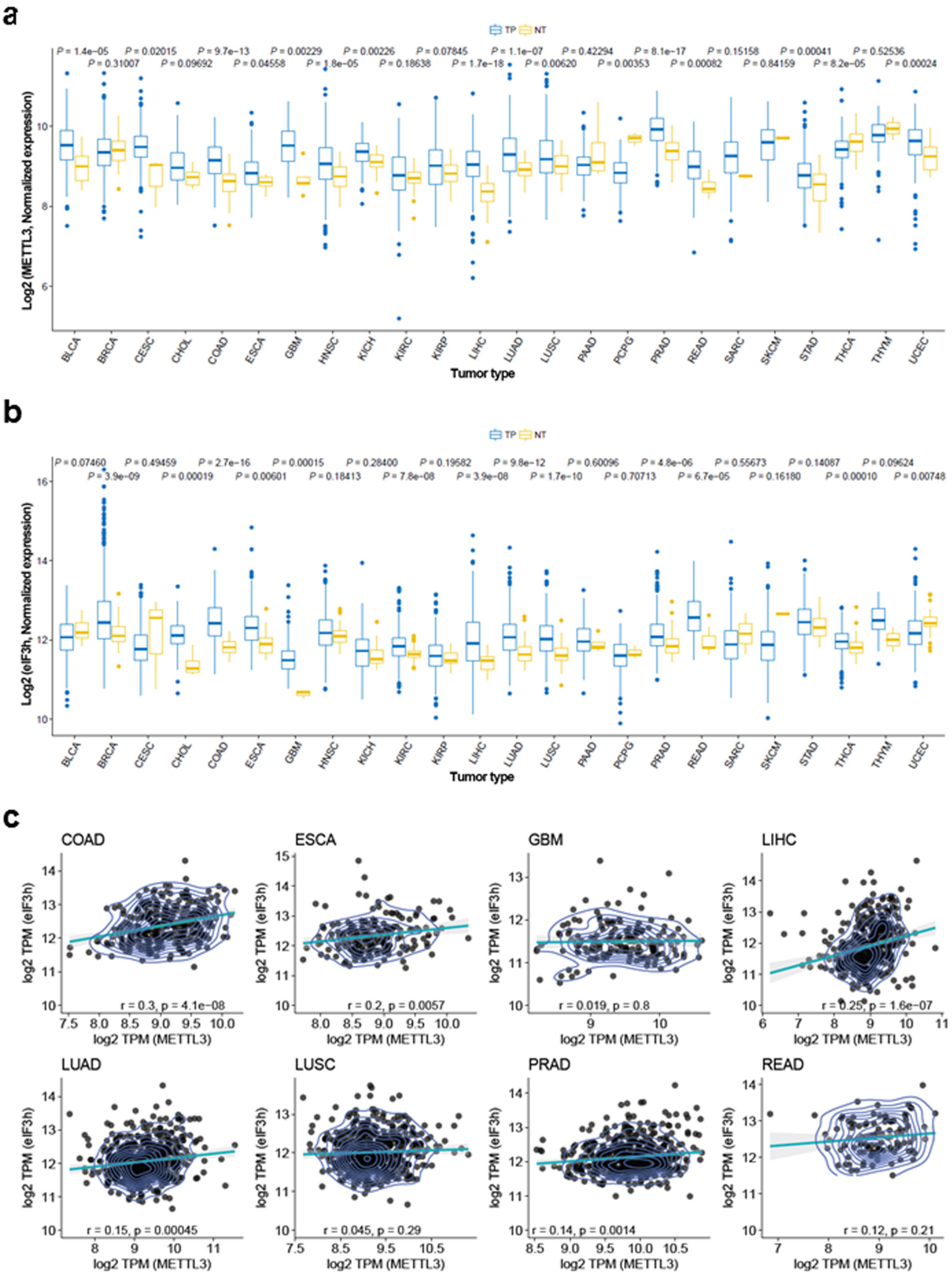


**Extended Data Fig. 10 | Expression of METTL3 and eIF3h is positively correlated in many tumour types. a**, *METTL3* gene expression among TCGA tumours. **b**, eIF3h gene expression among TCGA tumours. **a**, **b**, Box plots display the full range of variation on the basis of the five number summaries (minimum, first quartile, median, third quartile, and maximum). NT, solid tissue normal; TP, primary solid tumour. Two-sided Wilcoxon signed-rank test was used for statistical significance. **c**, Plot illustrating the Pearson's correlations of expression level between METTL3 and eIF3h in eight TCGA tumours, in which both METTL3 and eIF3h are significantly changed when compared with normal tissues.

nature research

Corresponding author(s): Richard I. Gregory

# Reporting Summary

Nature Research wishes to improve the reproducibility of the work that we publish. This form provides structure for consistency and transparency in reporting. For further information on Nature Research policies, see Authors & Referees and the Editorial Policy Checklist.

## Statistical parameters

When statistical analyses are reported, confirm that the following items are present in the relevant location (e.g. figure legend, table legend, main text, or Methods section).

| n/a | Confirmed | |
|---|---|---|
| ☐ | ☒ | The exact sample size (*n*) for each experimental group/condition, given as a discrete number and unit of measurement |
| ☐ | ☒ | An indication of whether measurements were taken from distinct samples or whether the same sample was measured repeatedly |
| ☐ | ☒ | The statistical test(s) used AND whether they are one- or two-sided<br>*Only common tests should be described solely by name; describe more complex techniques in the Methods section.* |
| ☐ | ☒ | A description of all covariates tested |
| ☐ | ☒ | A description of any assumptions or corrections, such as tests of normality and adjustment for multiple comparisons |
| ☐ | ☒ | A full description of the statistics including central tendency (e.g. means) or other basic estimates (e.g. regression coefficient) AND variation (e.g. standard deviation) or associated estimates of uncertainty (e.g. confidence intervals) |
| ☐ | ☒ | For null hypothesis testing, the test statistic (e.g. *F*, *t*, *r*) with confidence intervals, effect sizes, degrees of freedom and *P* value noted<br>*Give P values as exact values whenever suitable.* |
| ☒ | ☐ | For Bayesian analysis, information on the choice of priors and Markov chain Monte Carlo settings |
| ☒ | ☐ | For hierarchical and complex designs, identification of the appropriate level for tests and full reporting of outcomes |
| ☒ | ☐ | Estimates of effect sizes (e.g. Cohen's *d*, Pearson's *r*), indicating how they were calculated |
| ☐ | ☒ | Clearly defined error bars<br>*State explicitly what error bars represent (e.g. SD, SE, CI)* |

*Our web collection on statistics for biologists may be useful.*

## Software and code

Policy information about availability of computer code

| | |
|---|---|
| Data collection | To analyze METTL3 or eIF3h expression level among TCGA tumors, RNA-Seq data for TCGA tumor types were downloaded from Genomic Data Commons Data Portal (GDC) of TCGA (http://cancergenome.nih.gov/) using R package TCGAbiolinks. |
| Data analysis | For high throughput sequencing data analysis, reads were aligned against the human hg19 (GRCh37) reference genome using Tophat2, rMATS v3.2.5 was used to detect the splicing events and significant splicing differences between METTL3 knockdown and control samples; MACS2.1.0 was used for the peak calling in m6A peak identification; mRNA half-life was calculated using the RPKM generated by HTSeq. |

For manuscripts utilizing custom algorithms or software that are central to the research but not yet described in published literature, software must be made available to editors/reviewers upon request. We strongly encourage code deposition in a community repository (e.g. GitHub). See the Nature Research guidelines for submitting code & software for further information.

## Data

Policy information about availability of data

All manuscripts must include a data availability statement. This statement should provide the following information, where applicable:

- Accession codes, unique identifiers, or web links for publicly available datasets
- A list of figures that have associated raw data
- A description of any restrictions on data availability

The m6A MeRIP-Seq and RNA-seq data have been deposited in the Gene Expression Omnibus (GEO) under accession number GSE117299. Figures 2b, 2c, 2g, 4j, 4k, ED5b, ED6b, ED8j, ED8k, ED9b and ED9c have associated raw data.

# Field-specific reporting

Please select the best fit for your research. If you are not sure, read the appropriate sections before making your selection.

☒ Life sciences ☐ Behavioural & social sciences ☐ Ecological, evolutionary & environmental sciences

For a reference copy of the document with all sections, see nature.com/authors/policies/ReportingSummary-flat.pdf

# Life sciences study design

All studies must disclose on these points even when the disclosure is negative.

| | |
|---|---|
| Sample size | For IHC staining, 75 lung adenocarcinoma and the adjacent control samples were used. For the mouse study, 5 mice (A549 cells) or 8 mice (NIH-3T3 cells) were used for each group. Based on Student T test, for comparison between two groups, a sample size of 5 is effencient to calculate the statistical significance. |
| Data exclusions | In Figure ED3d-f, we performed Mass spectrometry of FLAG-METTL3 containing complexes and found numerous translation factors including Ribosomal proteins and translation initiation factors. By doing independent IP, we confirmed several translation factors and ribosomal proteins. However, repeated data are already presented in our previous study (Lin et al., Mol Cell 2016) and current study. Therefore we decided to exclude the Western blot data of FLAG-METTL3 co-IP. |
| Replication | In the Figure legend, we stated how many number of replications were performed. Where it is applicable, Shapiro-Wilk test and Q-Q plotting (quantile-quantile plot,) were performed prior to Student's two-tailed t-test to assess if the data plausibly came from a normal distribution. Where indicated, Wilcoxon signed-rank test was used. All attempts at replication were successful. |
| Randomization | The mice were randomly divided into three groups for the xenograft study to determine the oncogenic role of METTL3 in vivo. |
| Blinding | The investigators were blinded to group allocation in the IHC staining. |

# Reporting for specific materials, systems and methods

### Materials & experimental systems

| n/a | Involved in the study |
|---|---|
| ☒ | ☐ Unique biological materials |
| ☐ | ☒ Antibodies |
| ☐ | ☒ Eukaryotic cell lines |
| ☒ | ☐ Palaeontology |
| ☐ | ☒ Animals and other organisms |
| ☐ | ☒ Human research participants |

### Methods

| n/a | Involved in the study |
|---|---|
| ☒ | ☐ ChIP-seq |
| ☐ | ☒ Flow cytometry |
| ☒ | ☐ MRI-based neuroimaging |

## Antibodies

| | |
|---|---|
| Antibodies used | All antibodies used in the study are listed in Methods.<br>Here we state in order: Antibody name; (Company; Catalogue number; Source; Reactivity ; Dilution)<br>METTL3 (Proteintech; 15073-1-AP; Rabbit; Human, Mouse, Rat; 1:1000), (Abcam; ab195352; Rabbit; Mouse, Rat, Human; 1:1000)<br>β-actin (Abcam; ab8227; Rabbit; Mouse, Rat, Sheep, Rabbit, Chicken, Guinea pig, Cow, Dog, Human, Pig, Xenopus laevis, Drosophila melanogaster, Fish, Monkey, Zebrafish, Rhesus monkey, Chinese hamster; 1:5000) |

eIF3h (Abcam; ab60942; Mouse; Human; 1:1000)
CBP80 (Homemade; Rabbit; 1:5000)
CTIF (Homemade; Rabbit; 1:1000)
eIF4E (Cell Signaling Technology; #2067; Rabbit; Human, Mouse, Rat, Monkey; 1:1000)
eIF3b (Santa Cruz Biotechnology; sc-16377; Goat; Mouse, Rat, Human; 1:1000)
eIF4GI (Cell Signaling Technology; #2498; Rabbit; Human, Mouse, Rat, Monkey; 1:1000)
FLAG (Sigma; A8592; Mouse; FLAG-fusion protein; 1:5000)
BRD4 (Abcam; ab128874; Rabbit; Mouse, Rat, Human, 1:1000), (Cell signaling; #13440; Rabbit; Human; 1:1000)
CD9 (Cell Signaling Technology; #13174; Rabbit; Human; 1:1000)
MGMT (Cell Signaling Technology; #2739; Rabbit; Human, Monkey; 1:1000)
TIMP1 (Cell Signaling Technology; #8946; Rabbit; Human, Monkey; 1:1000)
FTO (Phosphosolution; 597-FTO; Moue; Rat, Mouse, Human; 1:1000)
Anti-Flag M2 Affinity Gel (Sigma-Aldrich; A2220; Mouse; FLAG-fusion protein; 1:200)
For PLA, Duolink® In Situ Red Starter Kit Mouse/Rabbit (Sigma-Aldrich; DUO92101; Mouse/Rabbit; Followed manufacturer's instruction)

Validation

The antibodies that have been validated by the supplyers for specific purposes (for example, western blot) were purchased for our experiment. In addition, for key essential antibodies such as METTL3, eIF3h antibodies, we further validated the antibodies by western blotting upon depletion of the proteins. For CBP80 and CTIF homemade antibodies, validation was performed in Choe et al., THE JOURNAL OF BIOLOGICAL CHEMISTRY 2012; VOL. 287, NO. 22, pp. 18500–18509.

## Eukaryotic cell lines

Policy information about cell lines

Cell line source(s)

All cell lines used in this study, including human lung cancer cell lines (A549 and H1299), HEK293T, BJ, NIH-3T3, HeLa and MEFs were purchased from ATCC.

Authentication

Cell lines were authenticated with morphology, karyotyping, and PCR based approaches by ATCC

Mycoplasma contamination

The cell lines were tested for potential mycoplasma contamination and confirmed that they are mycoplasma negative.

Commonly misidentified lines
(See ICLAC register)

No commonly misidentified cell lines were used in this study.

## Animals and other organisms

Policy information about studies involving animals; ARRIVE guidelines recommended for reporting animal research

Laboratory animals

All research involving animals was complied with protocols approved by the Beth Israel Deaconess Medical Center Institutional Animal Care and Use Committee. 4-6 weeks old female NU/J (Nude) immunodeficient mice (Jackson Laboratory #002019) were used for subcutaneous injections.

Wild animals

The study did not involve wild animals.

Field-collected samples

The study did not involve samples collected from the field.

## Human research participants

Policy information about studies involving human research participants

Population characteristics

Lung cancer tumor samples were isolated from four patients (Patient 1: Female, Age 73 mixed subtype, with acinar (10%), papillary (80%),and bronchioloalveolar (10%) patterns, moderately differentiated, 5.1cm; Patient 2: Male, Age 80, mixed subtype with 80% papillary, 14% acinar, 5% bronchioloalveolar, and 1% solid patterns, moderately differentiated, 8cm. Patient 3: Male, Age 79 with acinar (20%), papillary (60%), andbronchioloalveolar (20%) patterns, moderately differentiated, 5.0cm; Patient 4: Female, age 61, lung adenocarcinoma, micropapillary predominant, with solid, acinar and papillary areas, poorly differentiated, 10.5 cm).

Recruitment

lung adenocarcima samples from four patients (two males and two females) were used for the profiling of m6A modification in primary tumor tissues. Since this is a pilot study of m6A in primary lung cancer samples, we selected the patients with large size tumors so that we can get enough RNA samples for m6A profiling, there is no potential self-selection bias.

# Flow Cytometry

## Plots

Confirm that:

☒ The axis labels state the marker and fluorochrome used (e.g. CD4-FITC).

☒ The axis scales are clearly visible. Include numbers along axes only for bottom left plot of group (a 'group' is an analysis of identical markers).

☒ All plots are contour plots with outliers or pseudocolor plots.

☒ A numerical value for number of cells or percentage (with statistics) is provided.

## Methodology

| | |
|---|---|
| Sample preparation | METTL3 knockdown and control A549 cells were treated with 500nM JQ1 and then analyzed by Annexin V/PI staining using FACS. |
| Instrument | BD LSR II |
| Software | BD FACSDiva Software. |
| Cell population abundance | No sorting in this study. |
| Gating strategy | Gating was performed using three controls: Annexin V-/PI-, Annexin V+/PI-, Annexin V-/PI+. |

☒ Tick this box to confirm that a figure exemplifying the gating strategy is provided in the Supplementary Information.